ADA037077

TECHNICAL REPORT RD-77-8

THE EFFECTIVENESS OF CANARDS FOR ROLL CONTROL

James R. Burt, Jr.
Aeroballistics Directorate
US Army Missile Research, Development and Engineering Laboratory
US Army Missile Command
Redstone Arsenal, Alabama 35809

November 1976

Approved for public release; distribution unlimited.

U.S. ARMY MISSILE COMMAND
Redstone Arsenal, Alabama 35809

DISPOSITION INSTRUCTIONS

DESTROY THIS REPORT WHEN IT IS NO LONGER NEEDED. DO NOT RETURN IT TO THE ORIGINATOR.

DISCLAIMER

THE FINDINGS IN THIS REPORT ARE NOT TO BE CONSTRUED AS AN OFFICIAL DEPARTMENT OF THE ARMY POSITION UNLESS SO DESIGNATED BY OTHER AUTHORIZED DOCUMENTS.

TRADE NAMES

USE OF TRADE NAMES OR MANUFACTURERS IN THIS REPORT DOES NOT CONSTITUTE AN OFFICIAL INDORSEMENT OR APPROVAL OF THE USE OF SUCH COMMERCIAL HARDWARE OR SOFTWARE.

UNCLASSIFIED

SECURITY CLASSIFICATION OF THIS PAGE (When Data Entered)

REPORT DOCUMENTATION PAGE

READ INSTRUCTIONS BEFORE COMPLETING FORM

14

1. REPORT NUMBER: RD-77-8

2. GOVT ACCESSION NO.

3. RECIPIENT'S CATALOG NUMBER

9

4. TITLE (and Subtitle)

6

THE EFFECTIVENESS OF CANARDS FOR ROLL CONTROL

5. TYPE OF REPORT & PERIOD COVERED: Technical Rep[redacted]t,

6. PERFORMING ORG. REPORT NUMBER: RD-77-8

7. AUTHOR(s)

10

James R. Burt, Jr

8. CONTRACT OR GRANT NUMBER(s)

16

9. PERFORMING ORGANIZATION NAME AND ADDRESS

Commander
US Army Missile Command
ATTN: DRSMI-RD
Redstone Arsenal Ala 35809

10. PROGRAM ELEMENT, PROJECT, TASK AREA & WORK UNIT NUMBERS

DA 1W362303A214
AMCMS 63203.2140511.03

11. CONTROLLING OFFICE NAME AND ADDRESS

Commander
US Army Missile Command
ATTN: DRSMI-RPR
Redstone Arsenal Ala 35809

11

12. REPORT DATE: Nov[redacted]76

13. NUMBER OF PAGES: 65

14. MONITORING AGENCY NAME & ADDRESS (if different from Controlling Office)

12

65p.

15. SECURITY CLASS (of this report): UNCLASSIFIED

15a. DECLASSIFICATION/DOWNGRADING SCHEDULE

16. DISTRIBUTION STATEMENT (of this Report)

DDC

MAR 18

C

17. DISTRIBUTION STATEMENT (of the abstract entered in Block 20, if different from Report)

18. SUPPLEMENTARY NOTES

19. KEY WORDS (Continue on reverse side if necessary and identify by block number)

Roll control
Small, nose mounted canards
Clipped delta planform
Planar tail
Ring tail

20. ABSTRACT (Continue on reverse side if necessary and identify by block number)

A study of the roll control effectivness of small, nose mounted canards is presented. Mach number was varied from 0.6 to 4.5, canard differential deflection from -3° to 5°, and angle of attack from -3° to 6°. The canards were small with a clipped delta planform and were tested in two longitudinal nose positions in combination with both a planar tail and a ring tail. It is shown that the effectiveness of small, nose mounted canards as roll control devices depends upon tail shape.

DD FORM 1 JAN 73 1473 EDITION OF 1 NOV 65 IS OBSOLETE

UNCLASSIFIED

SECURITY CLASSIFICATION OF THIS PAGE (When Data Entered)

400407

HB

CONTENTS

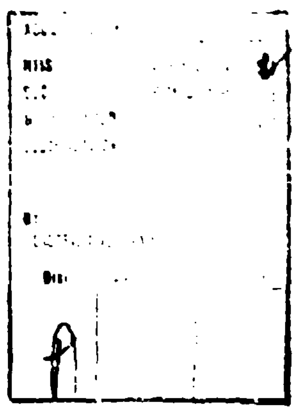

I. INTRODUCTION

Nose mounted canards are attractive candidates for aerodynamic controls on a guided missile for several reasons. Generally, the hinge moments are small compared to those developed by an equally effective tail control. The effectiveness of canards increases with increasing angle of attack rather than decreasing as does tail control effectiveness. Also canards may be employed to tailor the missile stability margin by decreasing the transonic stability hump [1].

A common requirement for a guided missile is that the roll rate should be maintained at a low level or even that the missile should be fixed in roll position. One potential advantage of nose mounted canards is that they may be considered as roll control devices as well as giving control forces for a maneuvering missile. The purpose of this study is to investigate the effectiveness of small, nose mounted canards in developing rolling moments for roll attitude and roll rate control.

The aerodynamics properties of canard-tail configurations are complicated by vortices, produced by the canards at incidence, trailing past the tail panels and effecting the tail lift. This phenomenon may be beneficial at times such as by increasing trim angle of attack for a given canard deflection angle or by decreasing the transonic static margin rise, thereby decreasing flight path errors due to wind sensitivity.

Theoretical predictions of the aerodynamics of canard-planar tail configurations are complicated by the difficulty in estimating correctly the canard induced vortex strengths and the vortex trajectories as they trail downstream past the tail panels. The method of Pitts, Nielsen, and Kaattari [2] was modified to calculate canard vortex induced planar tail rolling moments but comparison with experimental data was poor; therefore, it was not included in this report.

Wind tunnel data were obtained for canard-planar tail configurations with variable canard longitudinal positions. Mach number was varied from 0.6 to 4.5 and angle of attack and canard differential deflection was varied from -3° to 5°. The data were obtained from three different test facilities.

Some data were obtained for a canard-ring tail configuration at Mach numbers 2.5 and 4.5 with the canards located in only the most aft position. Comparisons are made between the canard-planar tail configurations and the canard-ring tail configuration in roll control effectiveness.

II. EXPERIMENTAL PROGRAM

A. Test Facilities

The 8-ft transonic wind tunnel, located at CALSPAN Corporation, Buffalo, New York, was used to obtain the data for Mach numbers of 0.6 to 1.25. The tunnel test section has perforated walls and an auxiliary pumping system for attenuation of reflected shock and expansion waves on models in the low supersonic range. This method of attenuating reflected shock and expansion waves is described in detail in Reference 3. The closed circuit tunnel is capable of speeds from 5 ft/sec up to Mach number 1.35. For this test, the tunnel was primarily run in a constant mass mode which is the most efficient way, timewise, to operate at several Mach numbers. Constant mass mode means that no air is added to the tunnel in going from one Mach number to another. In this mode, both Reynolds number and dynamic pressure vary with Mach number. A photograph of the installation is presented in Figure 1.

The Ames Research Center 6 ft X 6 ft supersonic wind tunnel was used to obtain data for Mach numbers 1.5 and 2.0. It is a closed-circuit, single-return, continuous-flow facility and has an asymmetric sliding-block nozzle and a test section with perforated floor and ceiling to permit boundary-layer removal. Continuous testing is available for Mach numbers from 0.25 to 2.25 with Reynolds numbers from 1.0×10^6 to 5.0×10^6/ft and a maximum stagnation temperature of 580°R. The tunnel air is driven by an eight-stage, axial-flow compressor powered by two electric motors mounted in tandem outside the wind tunnel. The Ames sting, EI III 235-500, together with a 5° angle adaptor, was used to mount the model. The model was inverted in the tunnel during all the tests.

The Arnold Engineering Development Center, Von Karmon Facility, Tunnel A, was used to obtain data for Mach numbers 2.5, 3.0, and 4.5. Tunnel A is a continuous, closed-circuit, variable density wind tunnel with an automatically driven flexible-plate nozzle and a 40 in. × 40 in. test section. The tunnel can be operated at Mach numbers from 1.5 to 6.0 at maximum stagnation pressures from 29 to 200 psia, respectively, and stagnation temperatures up to 750°R ($M_\infty = 6.0$). Minimum operating pressures range from approximately one-tenth to one-twentieth of the maximum at each Mach number. The tunnel is equipped with a model injection system which allows removal of the model from the test section while the tunnel remains in operation.

B. Wind Tunnel Model

The wind tunnel model was a sting mounted body of revolution, 5.0 in. diameter, 52.0 in. long, and had a three caliber tangent ogive. The model body is shown in Figure 2. The model was tested with two sets of canards, one set of planar tail panels and a ring tail. The model was unique in that all four canards and tail panels were each mounted on three component balances along with a six-component main balance which measured total model loads. Each canard was deflected remotely; the deflection angles were measured by potentiometers mounted on the canard deflection mechanism. The tail panels were undeflected throughout the tests.

C. Canards

The two sets of canards had essentially the same planform. These two sets were tested at two different longitudinal positions on the model nose with the canard root chord remaining tangent to the model surface at the canard hinge point. The two longitudinal positions are shown in Figure 3; the canards are shown in Figure 4.

D. Tail

A rectangular tail was tested with the trailing edge flush with the model base. The tail has an exposed aspect ratio of 1.0. A ring tail, designed to give approximately the same static stability as the planar tail was tested at Mach numbers 2.5 and 4.0. The vertical support struts were not attached to the body. With this arrangement, the two horizontal tail balances provided measurements of the total force on the ring tail. The tails are shown in Figure 4.

E. Test Conditions

The canard-planar tail configurations were tested at Mach numbers 0.6, 0.8, 0.9, 1.05, 1.25, 1.5, 2.0, 2.5, 3.0, and 4.5, while the ring tail configuration was tested only at Mach numbers 2.5 and 4.5. The angle of attack was varied from approximately -3° to 5° and the canards were deflected differentially from -3° to 5°. All data were corrected for sting deflections and flow angularities. Tunnel operating conditions are given in Table 1. The main balance accuracy was estimated to be 0.5% of full scale for each balance gage and the panel balance accuracies were estimated to be on the order of 1% of full scale, where the full scale loads are:

	Canard	Tail
Normal force (lb)	40	60
Root bending moment (in.-lb)	35	130
Hinge moment (in.-lb)	25	100

TABLE 1. TUNNEL OPERATING CONDITIONS

Mach Number	Reynolds No. × 10^{-6}/in.	Dynamic Pressure (psf)
0.6	0.16	460
0.8	0.17	500
0.9	0.18	420
1.05	0.19	490
1.25	0.21	550
1.5	0.20	500
2.0	0.20	500
2.5	0.23	547
3.0	0.26	547
4.5	0.40	547

It was estimated that angle of attack was accurate to ±0.05° and canard deflection angles to ±0.10°. The basic wind tunnel data are presented in plotted form in References 4, 5, and 6. The data axis system is shown in Figure 5.

F. Data Reduction

Total model rolling moment coefficient was calculated from the canard and tail balance data in the following manner:

$$C_{M_{R_C}} = -C_{M_{B_{C1}}} + C_{M_{B_{C2}}} + C_{M_{B_{C3}}} - C_{M_{B_{C4}}}$$

$$+ \frac{R_C}{D}\left(-CN_{C1}\cos\delta_{C1} + CN_{C2}\cos\delta_{C2} + CN_{C3}\cos\delta_{C3}\right.$$

$$\left. - CN_{C4}\cos\delta_{C4}\right)$$

$$C_{M_{R_T}} = -C_{M_{B_{T1}}} - C_{M_{B_{T2}}} + C_{M_{B_{T3}}} + C_{M_{B_{T4}}}$$

$$+ \frac{R_T}{D}\left(-CN_{T1} - CN_{T2} + CN_{T3} + CN_{T4}\right) .$$

Total rolling moment coefficient is:

$$C_{M_R} = C_{M_{R_C}} + C_{M_{R_T}} .$$

III DISCUSSION AND RESULTS

A. Canard-Tail Configuration Aerodynamics

The aerodynamic characteristics of canard-tail configurations are complex because the canards at incidence generate vortices which trail downstream past the tail and significantly change the tail lift. Vortex characteristics such as number of vortices, strength, position, and type are often difficult to predict analytically. At moderate angles of attack, the body may even generate symmetrical or unsymmetrical vortices which change the flow field about the tail panels and affect tail lift. Spahr and Dickey [7] have shown that the geometry of the wake as it leaves the canard or wing varies considerably with canard aspect ratio and angle of attack. The vortex sheet generated by low aspect ratio canard with subsonic leading edge tends to roll up into a single vortex ahead of the trailing edge; however, the vortex wake generated by a large aspect ratio canard at large angles of attack and with a supersonic leading edge may leave the trailing edge as a vortex sheet which rolls up into two vortices at some point downstream of the canard. The following sketch shows these two possibilities:

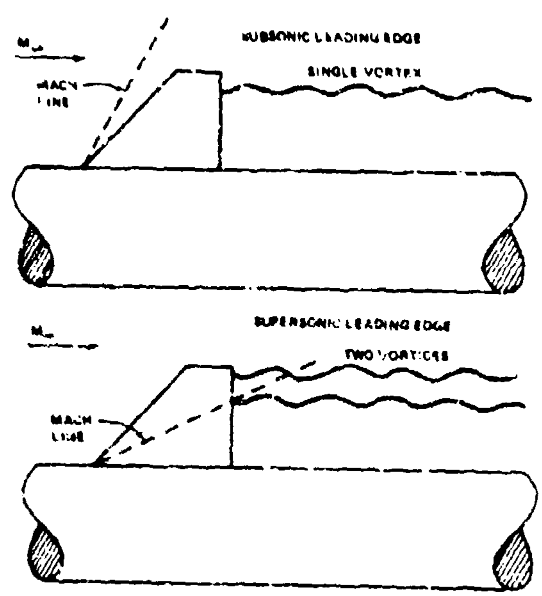

The canards used in this investigation all had subsonic leading edges and the series of vapor screen photographs in Figure 6 shows that one vortex is shed from each canard and appears to be completely rolled up as it leaves the canard trailing edge. The series of vapor screen photographs were taken at an angle of attack of 12°, sufficiently large for the body induced vortices to be generated as shown in the photographs.

B. Observations from Experimental Data

Wind tunnel tests were conducted in which opposite side canards were deflected differentially over the range -3° to 5° such that each canard produced a rolling moment in the same direction about the model centerline. Angle of attack was varied between -3° and 5° at each canard and Mach number condition.

C. Planar Tail

Figures 7 through 24 show rolling moment coefficient as a function of Mach number and angle of attack for a constant 5° differential canard deflection with the canards in the forward and aft position. These plots show the rolling moment coefficient developed by the canards only, the tails only, and the canards plus tail or total rolling moment coefficient. Total rolling moment coefficient measured directly from the model main balance is also shown and generally compares very well with the values computed from canard and tail balances.

The most notable aspect of the planar tail configuration data is that while the rolling moment developed by the canards is large, and that developed by the tail is large, the summed rolling moment coefficient is small because the direction or sign of the canard and tail values are different. The canard rolling moment coefficients are generated by the deflection angle of the four canards; however, the tail rolling moment coefficients are caused by the vortices, shed by the deflected canards, trailing past the tail panels and inducing an effective angle of attack for each tail panel. The canard rolling moments are generally larger than the tail rolling moments coefficients, but at the supersonic Mach numbers, the tail moment may be larger than the canard moment. In this case, the resultant moment is in the opposite direction than would be logically expected with the given canard deflection. This phenomenon has been termed roll reversal and is seen from the panel data at Mach numbers 1.05 and 2.0 with the canards in the forward position and Mach numbers 1.5 through 2.5 with the canards in the aft position. No data were obtained for the forward canard positions at Mach number 4.5. Roll reversal has been observed previously in wind tunnel tests of models with large canards located on the same body diameter as the planar tail.

Total rolling moment coefficient from the model main balance, planar tail configuration, is shown plotted on an expanded scale in Figures 25 through 42. At times, sizeable rolling moments were seen

in the data when all four canards were undeflected; those moments were subtracted from the data for deflected canards. This type of data correction is satisfactory if the zero deflection moments represent a constant bias in the data; however, this data adjustment is not correct if the zero deflection moments are due to a canard deflection bias error. A constant canard or tail deflection bias error would create a nonlinear error in rolling moment.

The expanded scale rolling moment data are shown plotted for the forward and aft mounted canard configurations throughout the canard deflection and Mach number range. The data are generally not symmetrical about zero angle of attack as would be expected for the configurations tested. The reason for this asymmetry is not known; however, Figures 7 through 42 showing the rolling moment component data indicate that the asymmetry is due to the tail component rather than the canard component. A slight misalignment of one or more of the tail panels may be the culprit; because, as previously stated, errors due to panel misalignment would be nonlinear with angle of attack. The rolling moments are generally in the expected direction subsonically and transonically, but in the supersonic Mach number range, the rolling moments are in the reverse direction than would be expected for both the configurations tested. The reason for this is not known other than the physical fact that the component of rolling moment due to the tail panels is larger than the component due to the canards. Roll reversal is clearly shown in Figure 43 for zero angle of attack and differential canard deflections of 5°.

D. Ring Tail

Figures 44 and 45 show rolling moment coefficients for the ring tail configuration as calculated from the canard balances alone, the tail alone, the canard-tail balance combination, and the main balance. These figures show that the ring tail, unlike the planar tail, does not develop large induced rolling moments at the Mach numbers tested. Because of this fact, small canards in combination with a ring tail appear to be far more effective as a means of roll control than small canards in line with an equivalent planar tail. Variation of rolling moment coefficient from the main balance as a function of angle of attack and canard deflection angle for the ring tail configuration is shown in Figures 46 and 47. Rolling moment coefficient for the ring tail configuration is a linear function of canard differential deflection and does not vary with angle of attack as does the planar tail configuration over the parameter ranges tested. A comparison of rolling moments from the planar tail and ring tail are shown in Figures 48 and 49. The ring tail configuration does have the possible disadvantage of increasing the missile drag from that of a planar tail configuration with approximately the same characteristics. The drag increase is shown in Figure 50.

IV. SUMMARY AND CONCLUSIONS

This report is a study of effectiveness of small nose mounted canards as roll control devices, moderate canard deflection angle, and small angles of attack. Wind tunnel data were obtained for canards in two different longitudinal positions. Mach number was varied from 0.6 to 4.5, canard differential deflection angle from -3° to 5°, and angle of attack from -3° to 6°.

The following conclusions were drawn from this study. Small, nose mounted canards in combination with an in-line planar tail are not effective as roll control devices unless decoupled from the tail panels because the vortex induced tail rolling moments are of the same magnitude as the rolling moments developed by the canards alone. The net rolling moments are generally only approximately 10% as large as the rolling moments developed by the canards alone. In the supersonic Mach number range, the tail component of rolling moments may actually be larger than the canard component, and in the opposite direction, leading to the condition known as roll reversal.

Small, nose mounted canards in combination with a ring tail, however, show promise as roll control devices because the canard induced vortices do not cause any significant tail rolling moments. A ring tail giving approximately the same stability characteristics as a planar tail does, however, cause some increase in total missile drag.

It is recommended that further wind tunnel tests be conducted in the subsonic and transonic Mach number range to supplement the rather small amount of canard-ring tail configuration data available. Variations in ring tail planform and mounting strut design should be included in these tests.

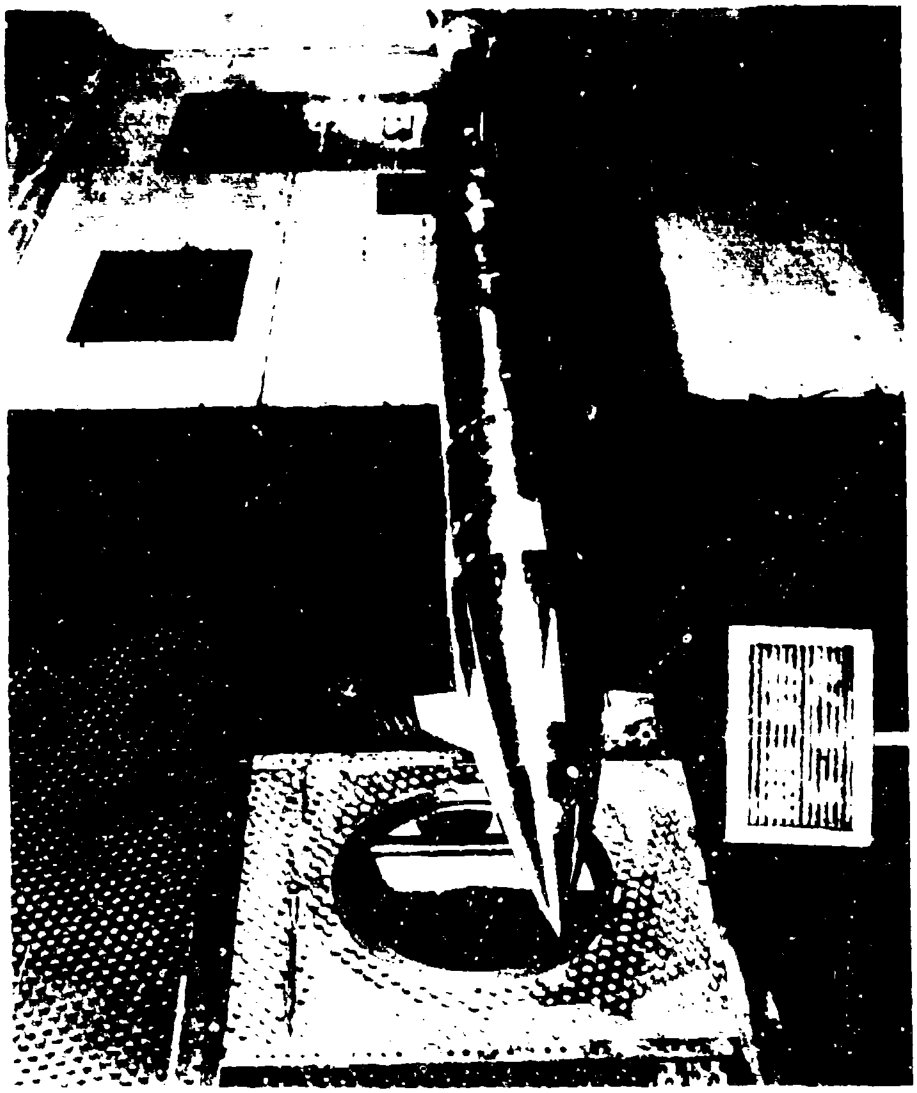

Figure 1. Typical model installation.

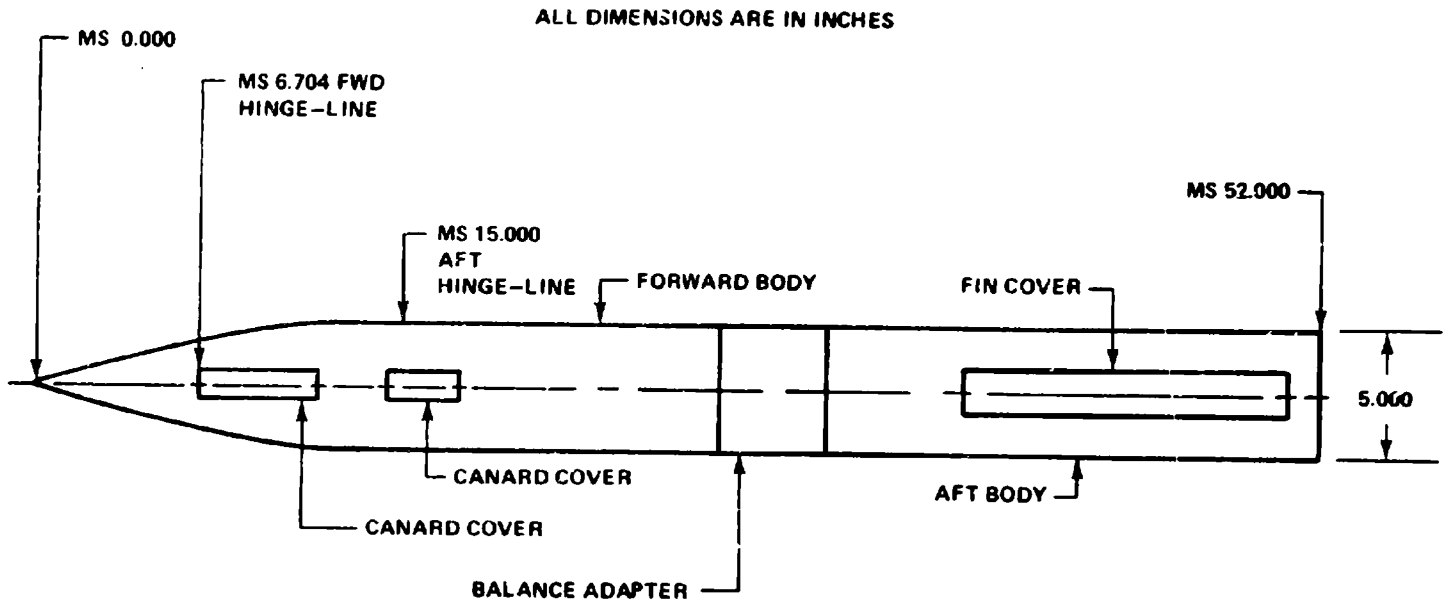

Figure 2. Sketch of model body showing hinge-line positions for canards.

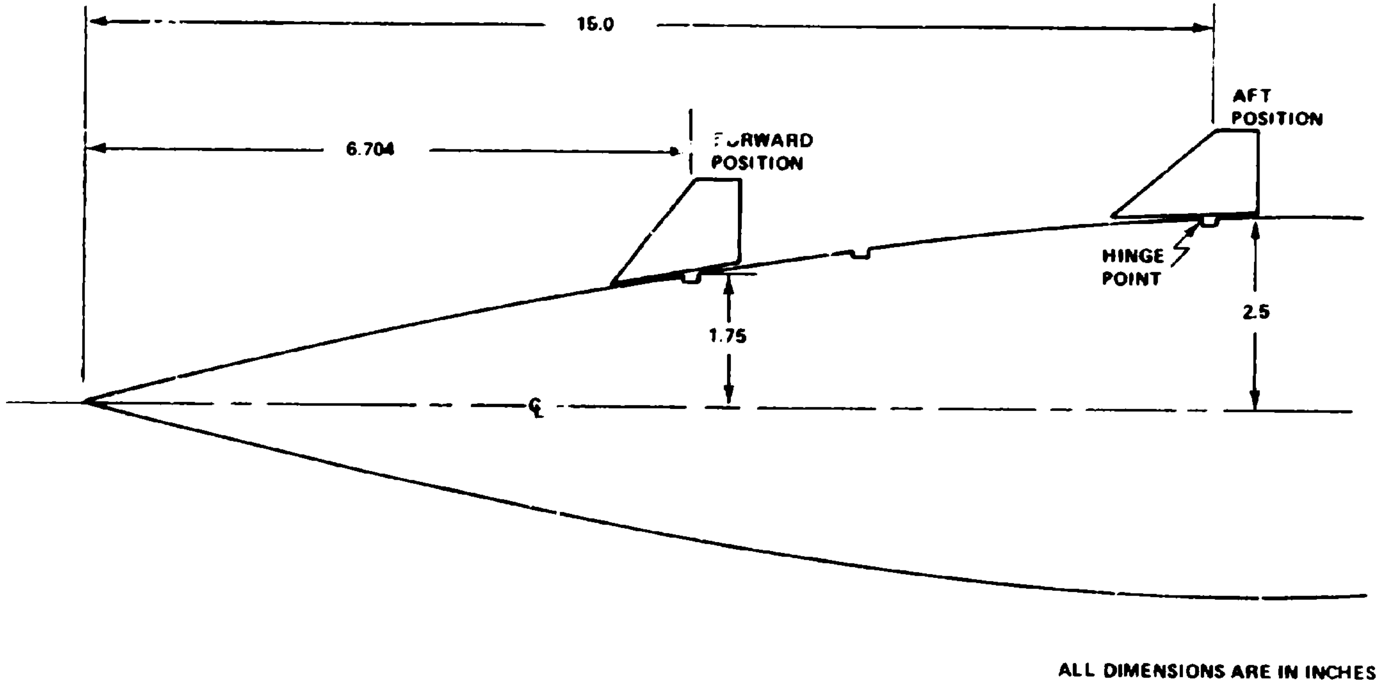

Figure 3. Canard longitudinal positions.

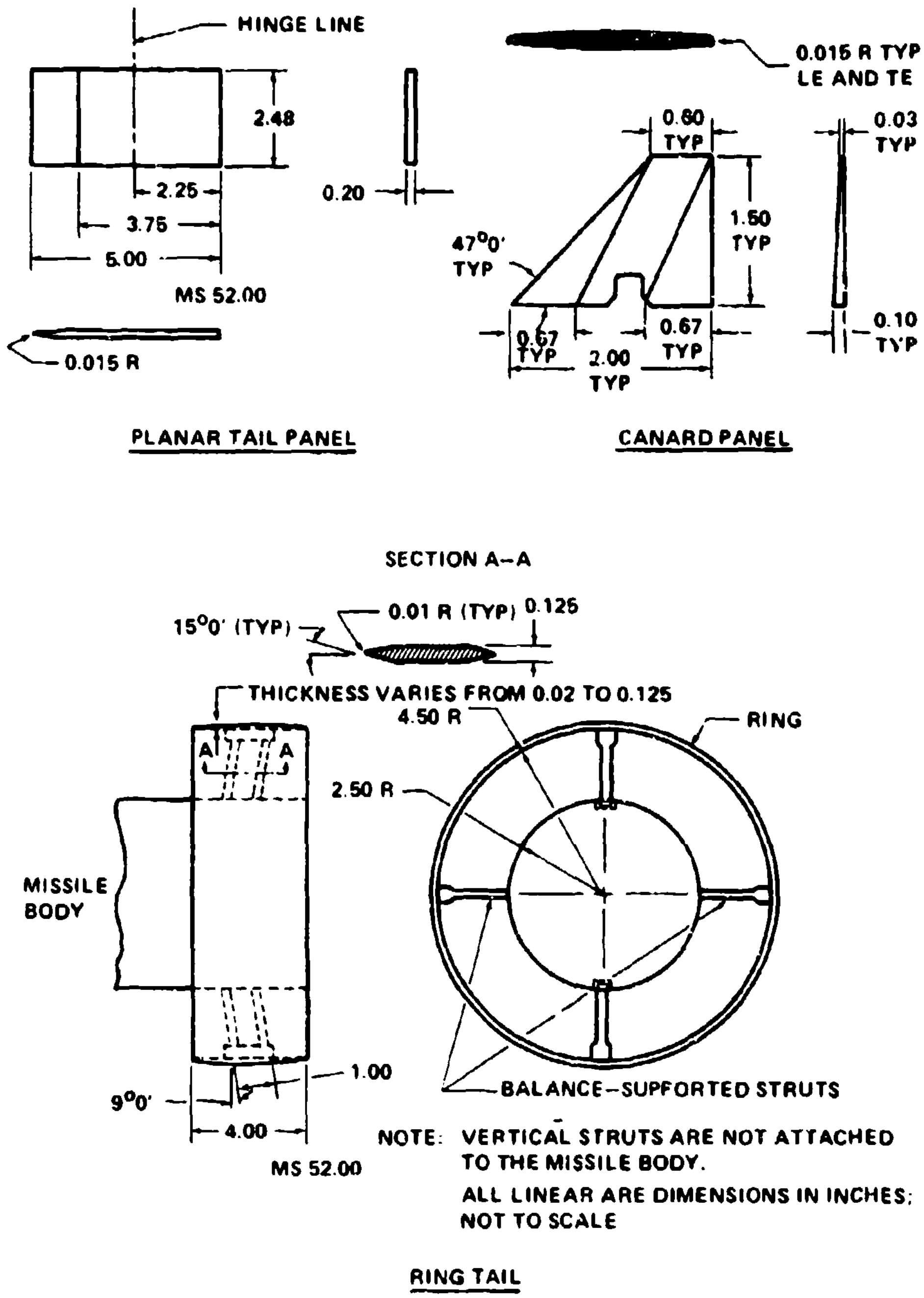

Figure 4. Planar tail, ring tail, and canard panel.

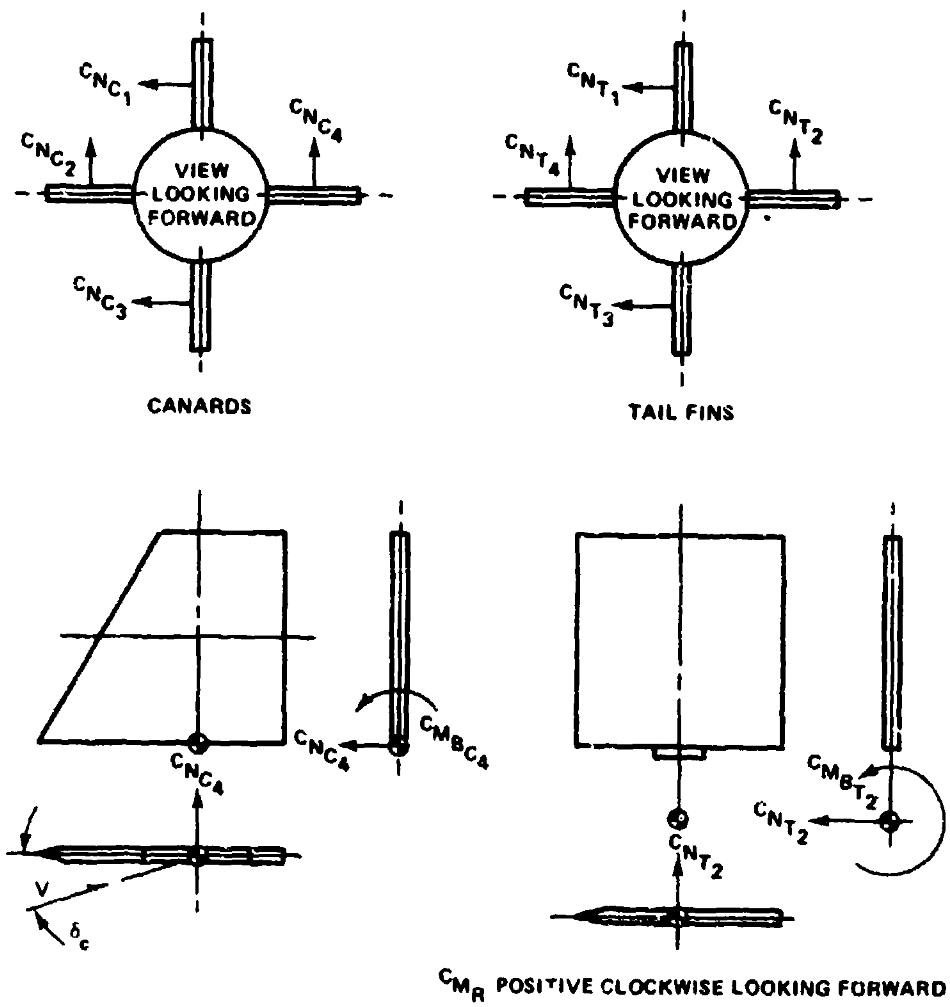

Figure 5. Axis system and positive sign convention (typical).

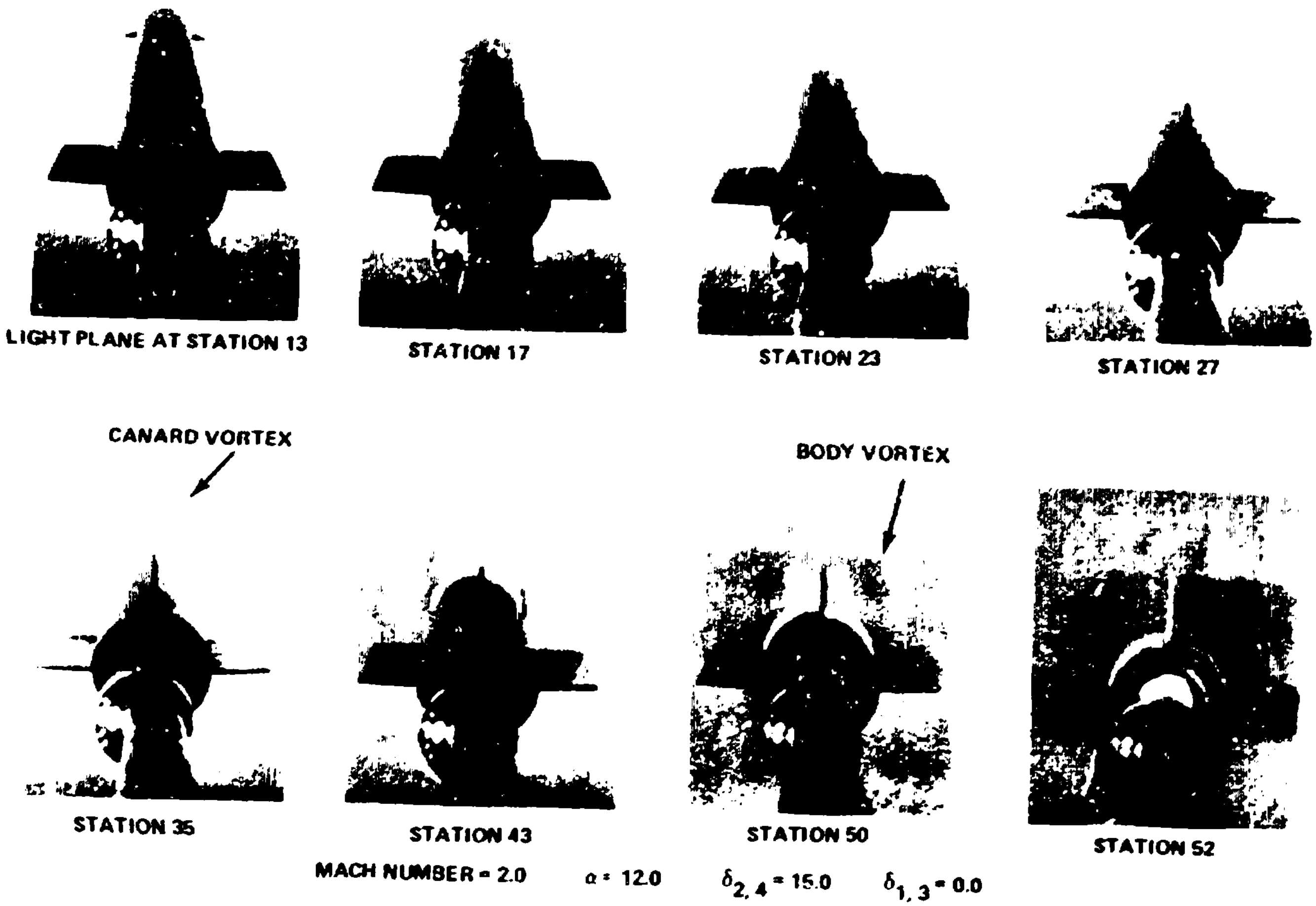

Figure 6. Typical vapor screen photographs.

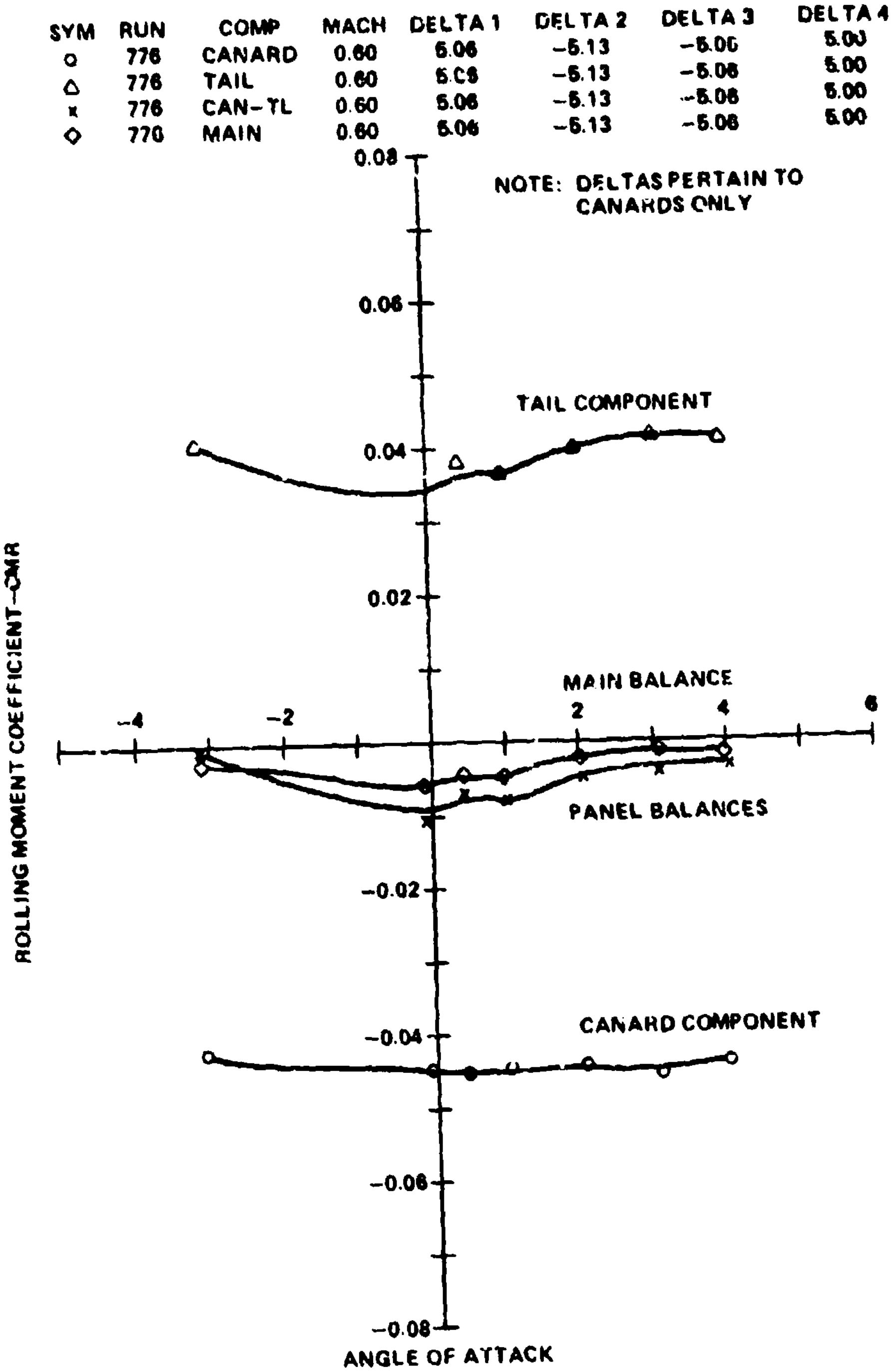

Figure 7. Component rolling moment coefficient, M_∞ = 0.6, forward canards, planar tail.

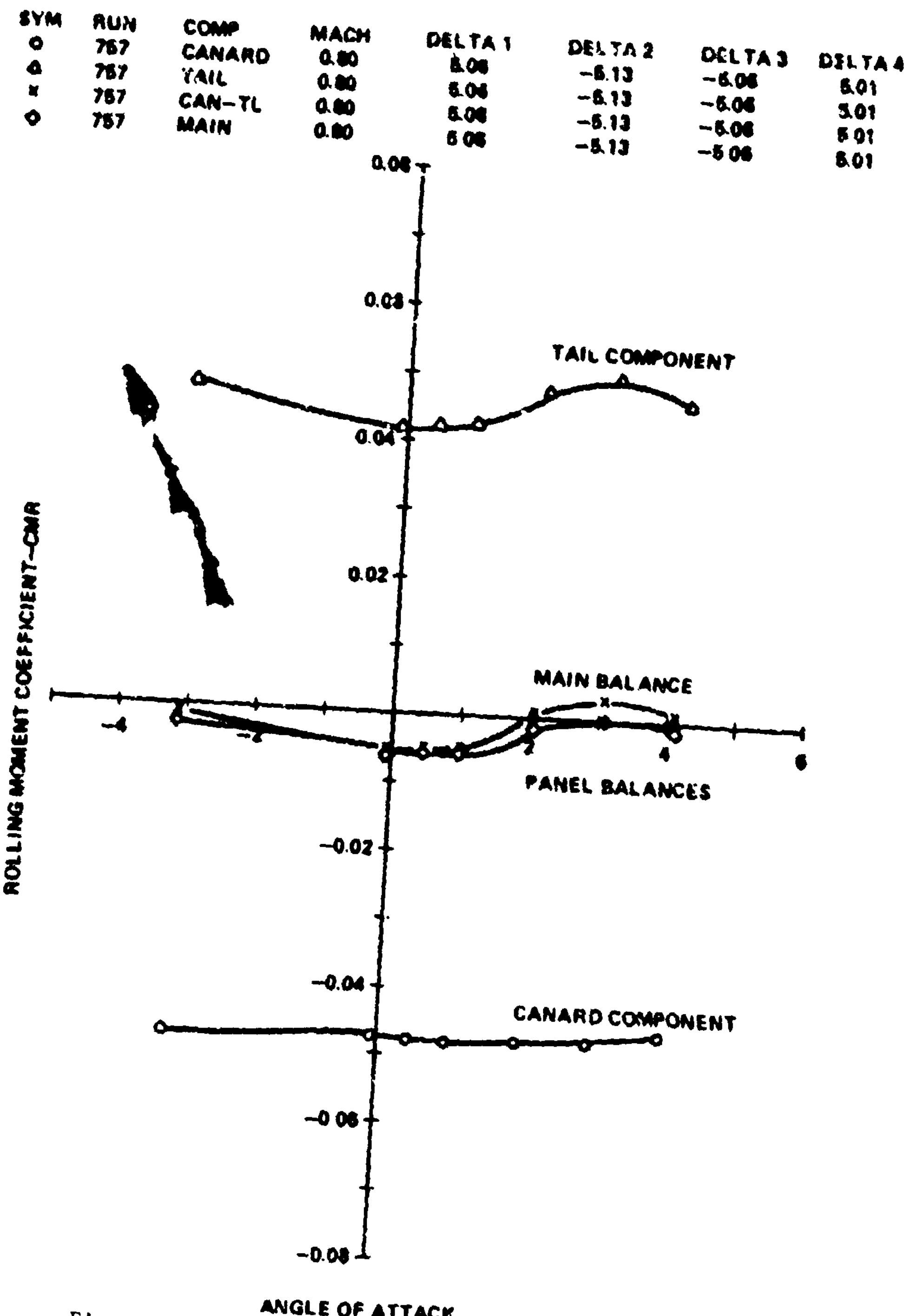

Figure 8. Component rolling moment coefficient, $M_{\infty} = 0.8$, forward canards, planar tail.

SYM	RUN	COMP	MACH	DELTA 1	DELTA 2	DELTA 3	DELTA 4
o	701	CANARD	0.90	5.06	-5.11	-5.05	5.02
Δ	701	TAIL	0.90	5.06	-5.11	-5.05	5.02
x	701	CAN-TL	0.90	5.06	-5.11	-5.05	5.02
◇	701	MAIN	0.90	5.06	-5.11	-5.05	5.02

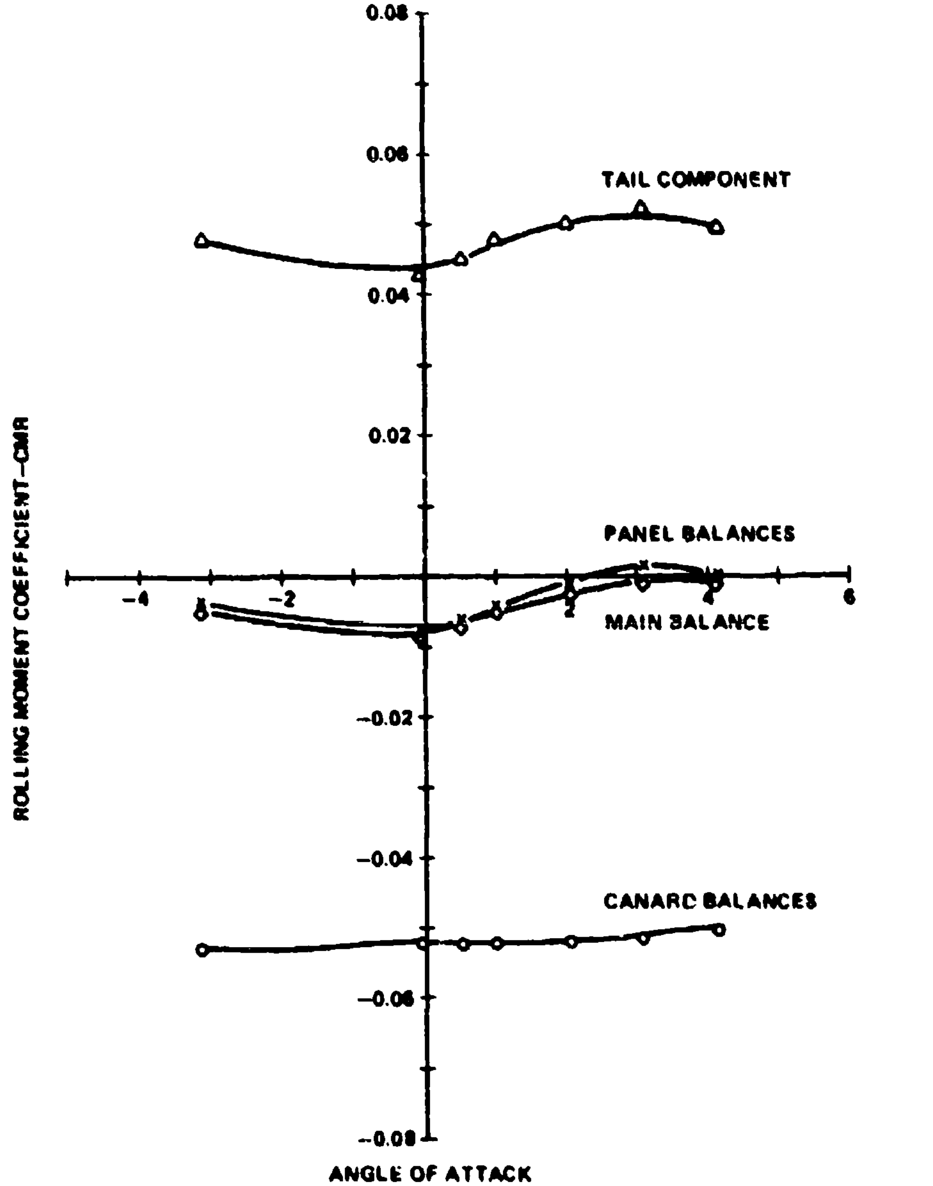

Figure 9. Component rolling moment coefficient, $M_\infty = 0.9$, forward canards, planar tail.

SYM	RUN	COMP	MACH	DELTA 1	DELTA 2	DELTA 3	DELTA 4
○	670	CANARD	1.05	5.07	−5.12	−5.06	5.01
△	670	TAIL	1.05	5.07	−5.12	−5.06	5.01
×	670	CAN−TL	1.05	5.07	−5.12	−5.06	5.01
◇	670	MAIN	1.05	5.07	−5.12	−5.06	5.01

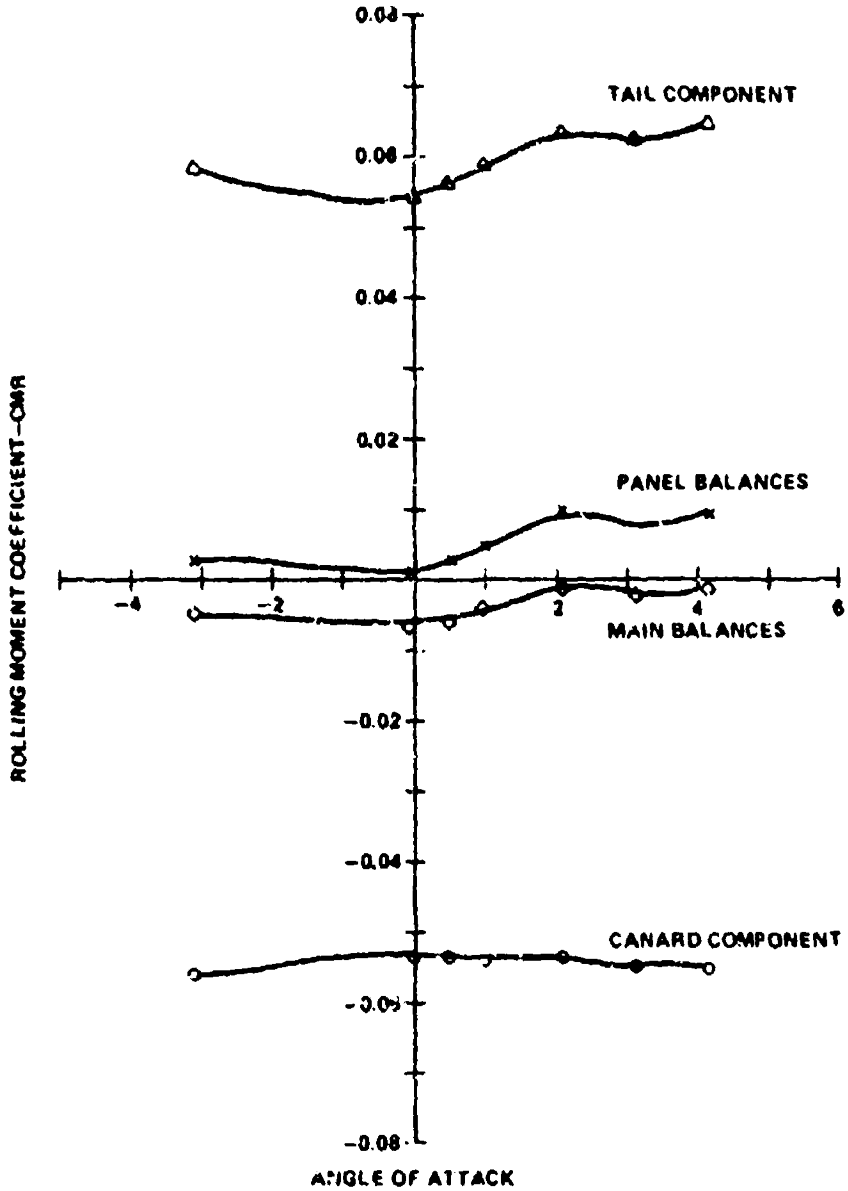

Figure 10. Component rolling moment coefficient, M_∞ = 1.05, forward canards, planar tail.

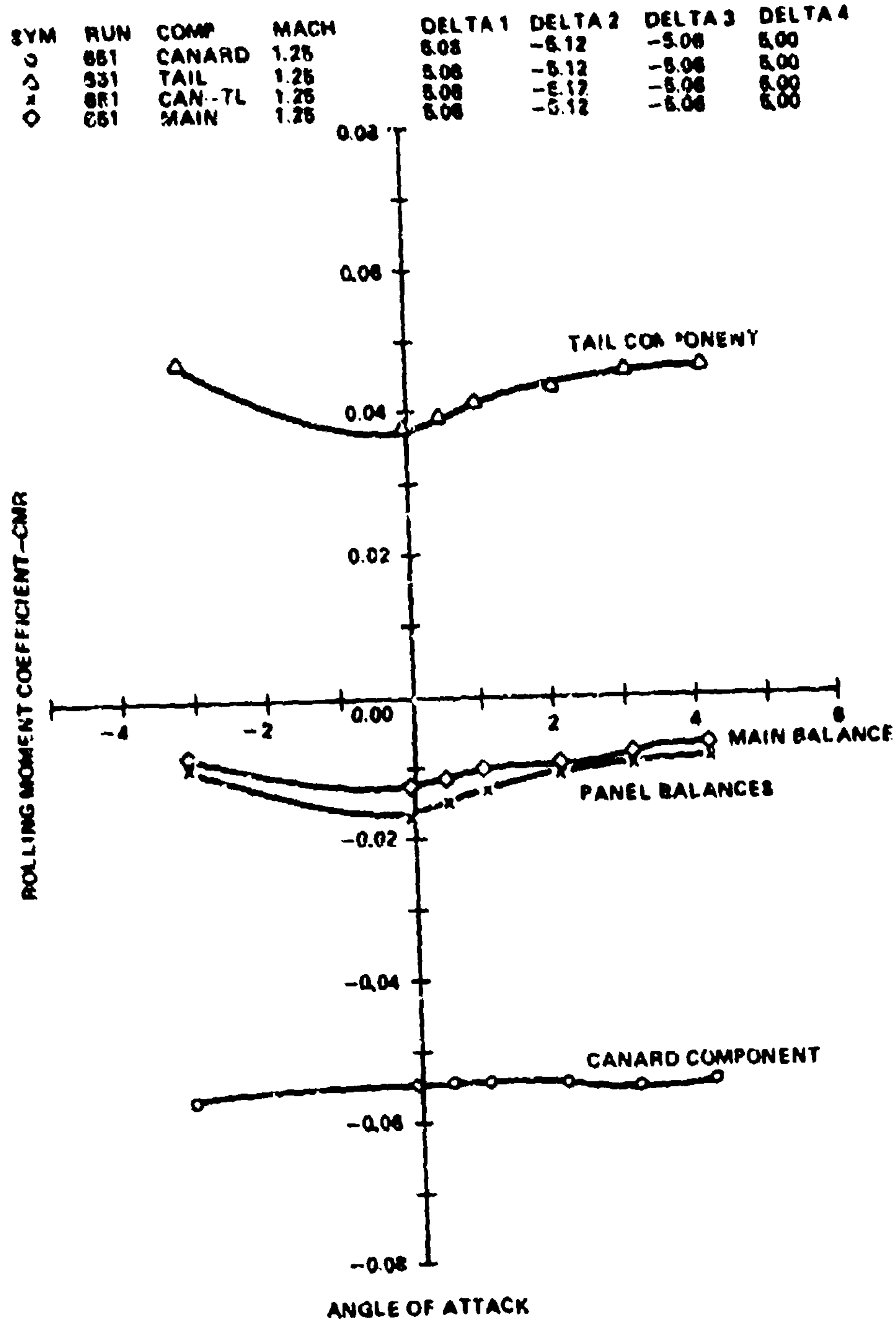

Figure 11. Component rolling moment coefficient, $M_\infty = 1.25$, forward canards, planar tail.

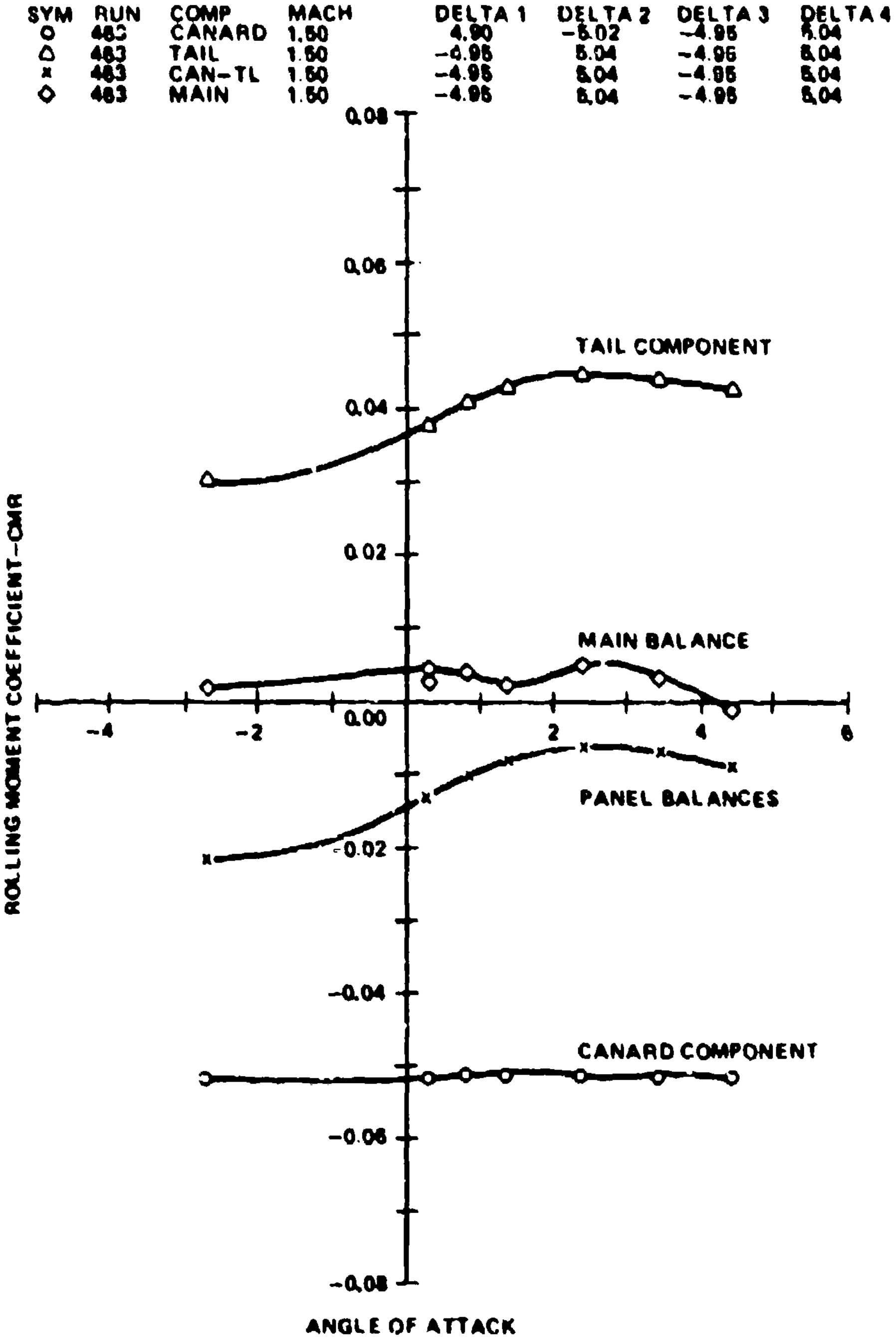

Figure 12. Component rolling moment coefficient, $M_\infty = 1.5$, forward canards, planar tail.

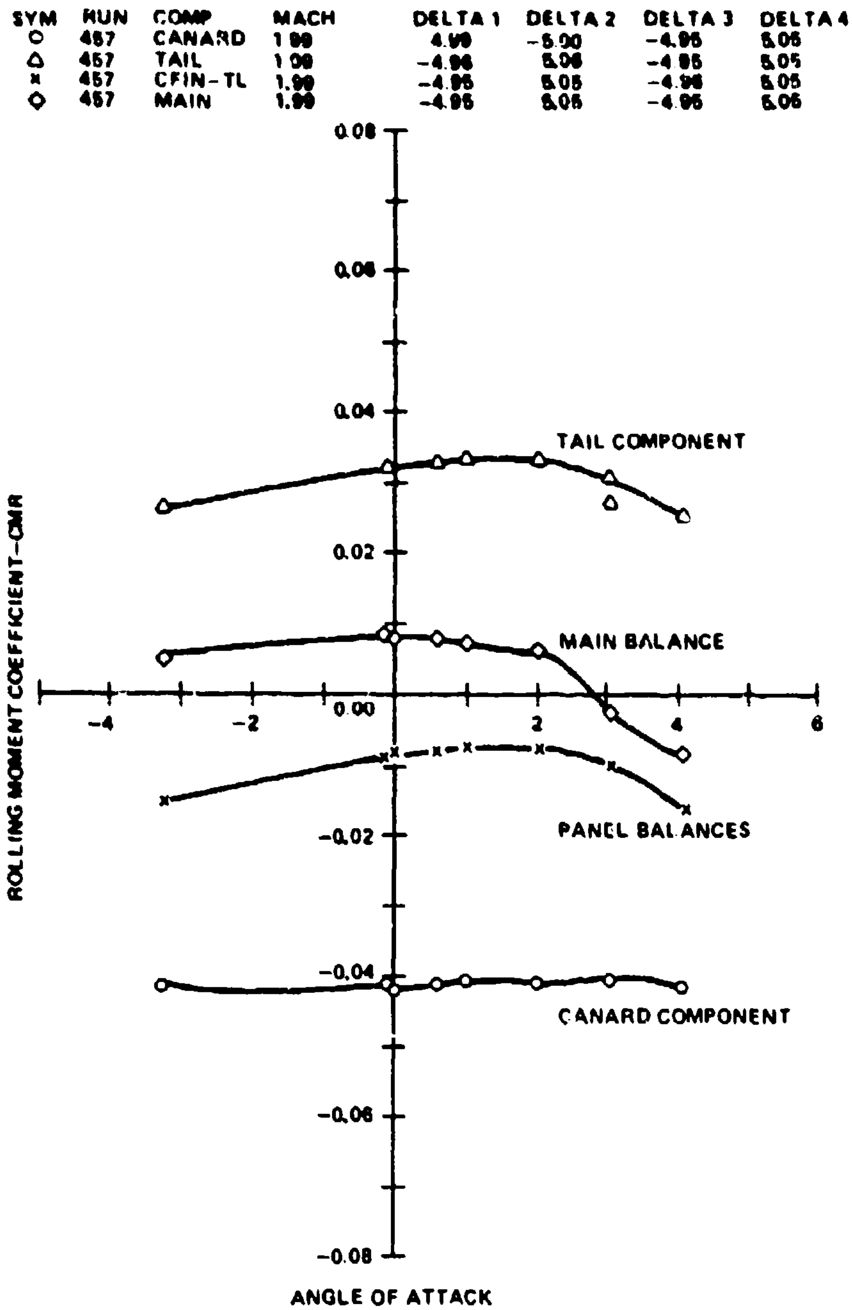

Figure 13. Component rolling moment coefficient, $M_{\infty} = 2.0$, forward canards, planar tail.

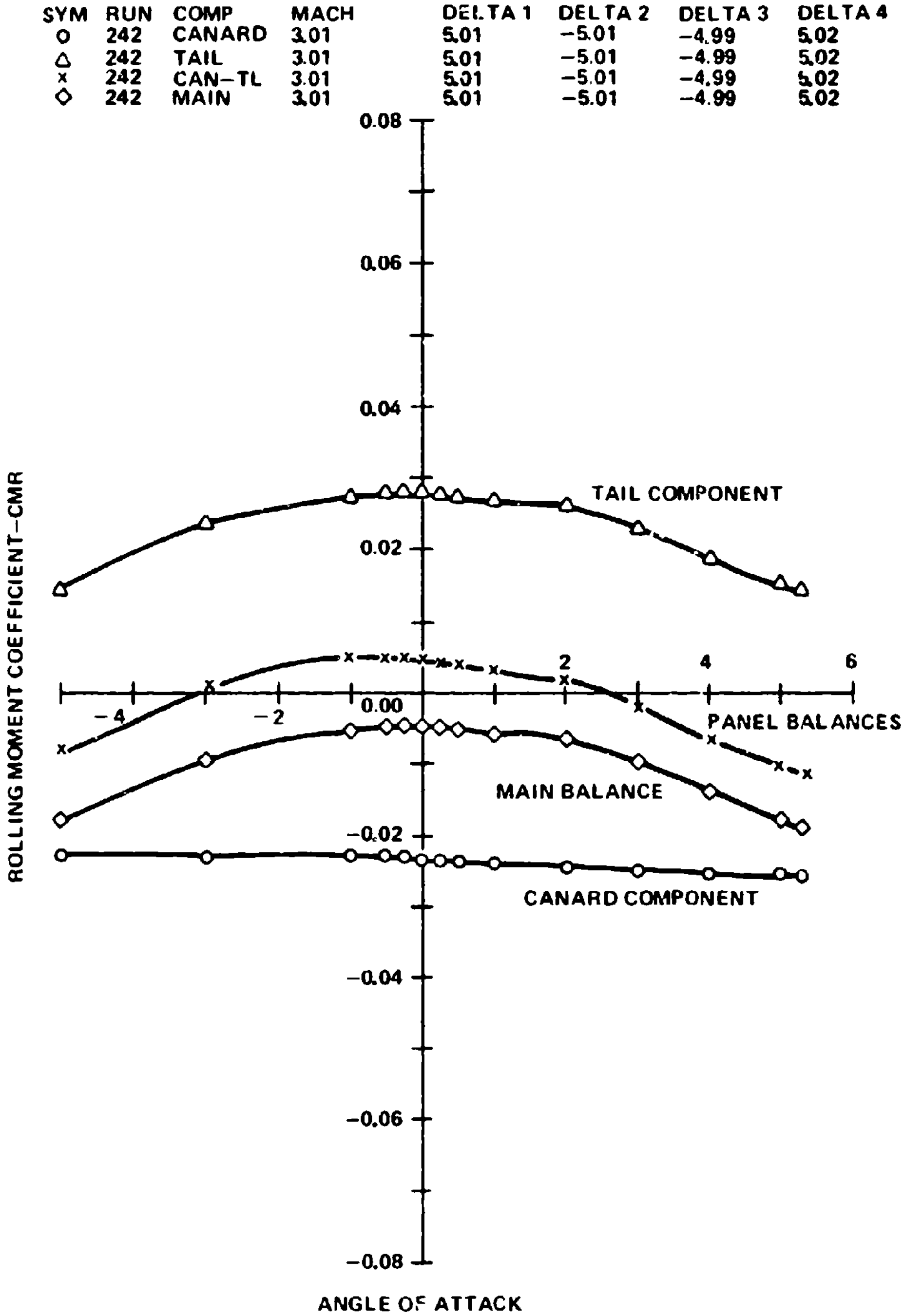

Figure 14. Component rolling moment coefficient, $M_\infty = 3.0$, forward canards, planar tail.

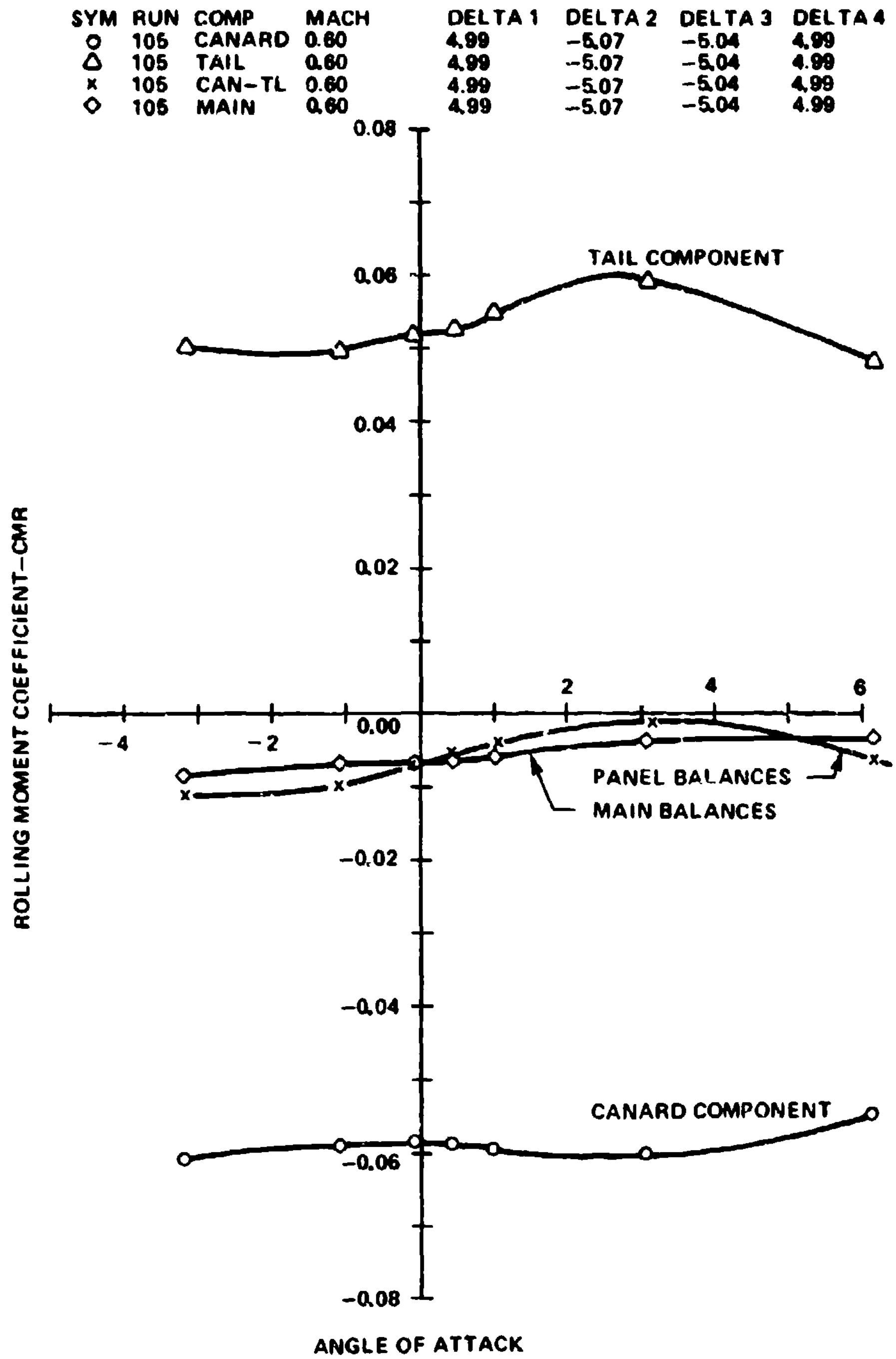

Figure 15. Component rolling moment coefficient, $M_{\infty} = 0.6$, aft canards, planar tail.

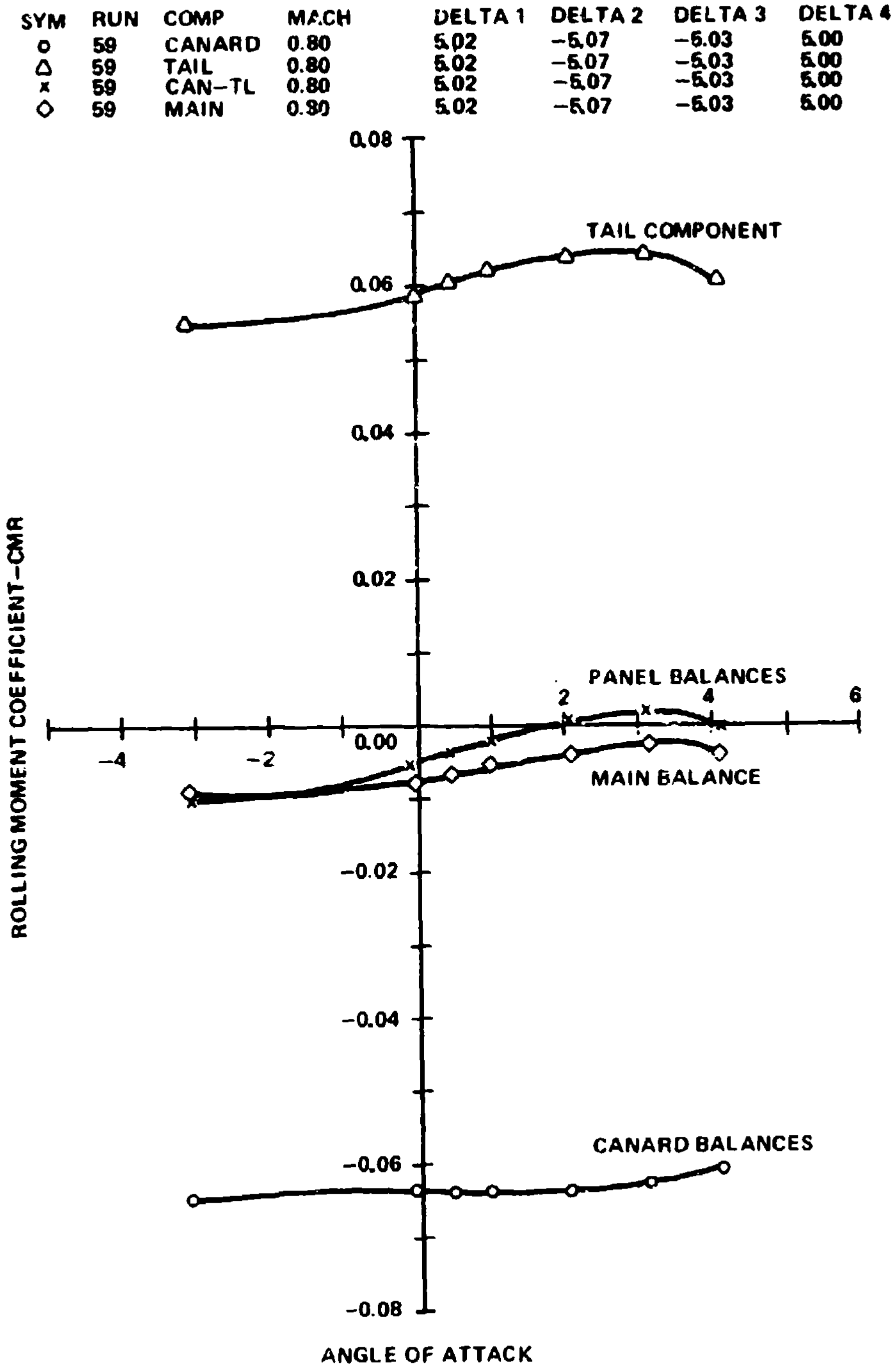

Figure 16. Component rolling moment coefficient, $M_\infty = 0.8$, aft canards, planar tail.

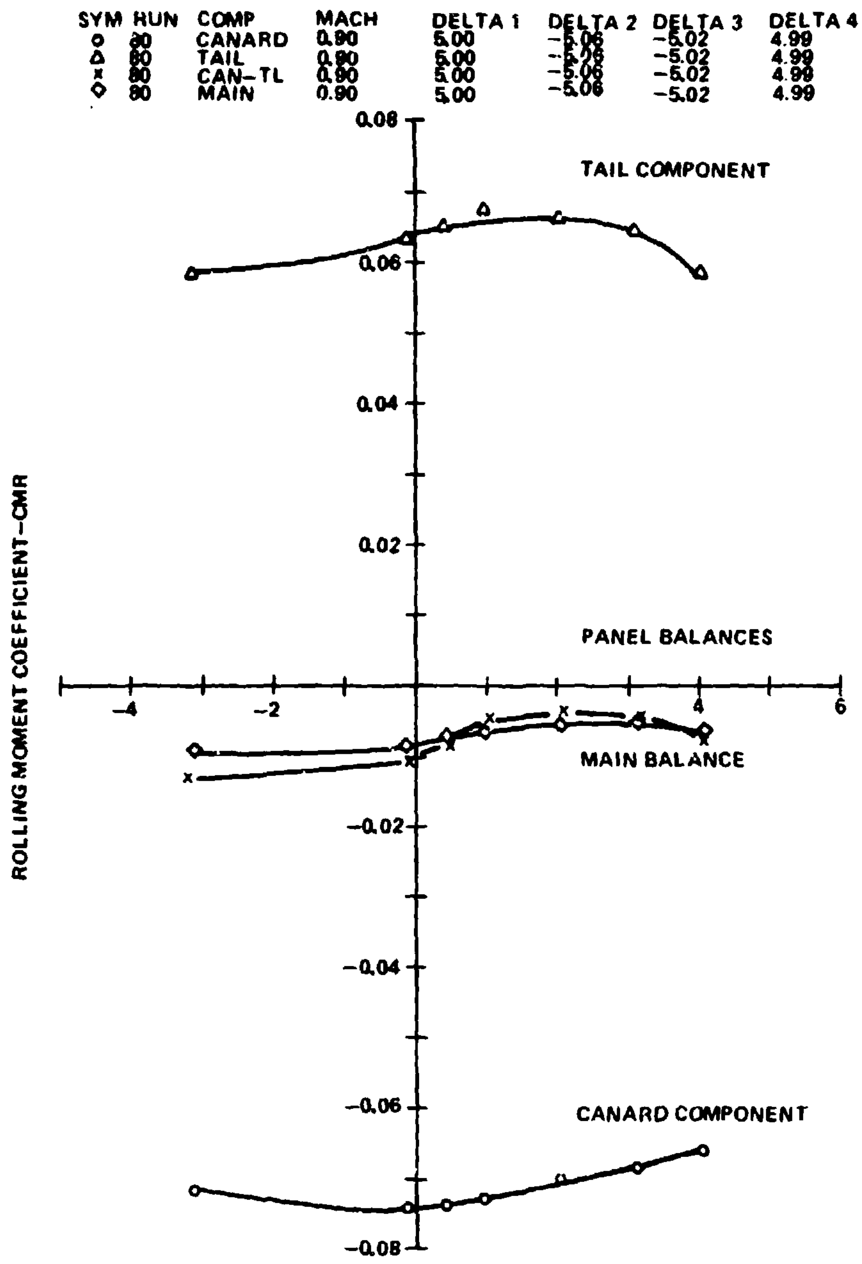

Figure 17. Component rolling moment coefficient, M_α = 0.9, aft canards, planar tail.

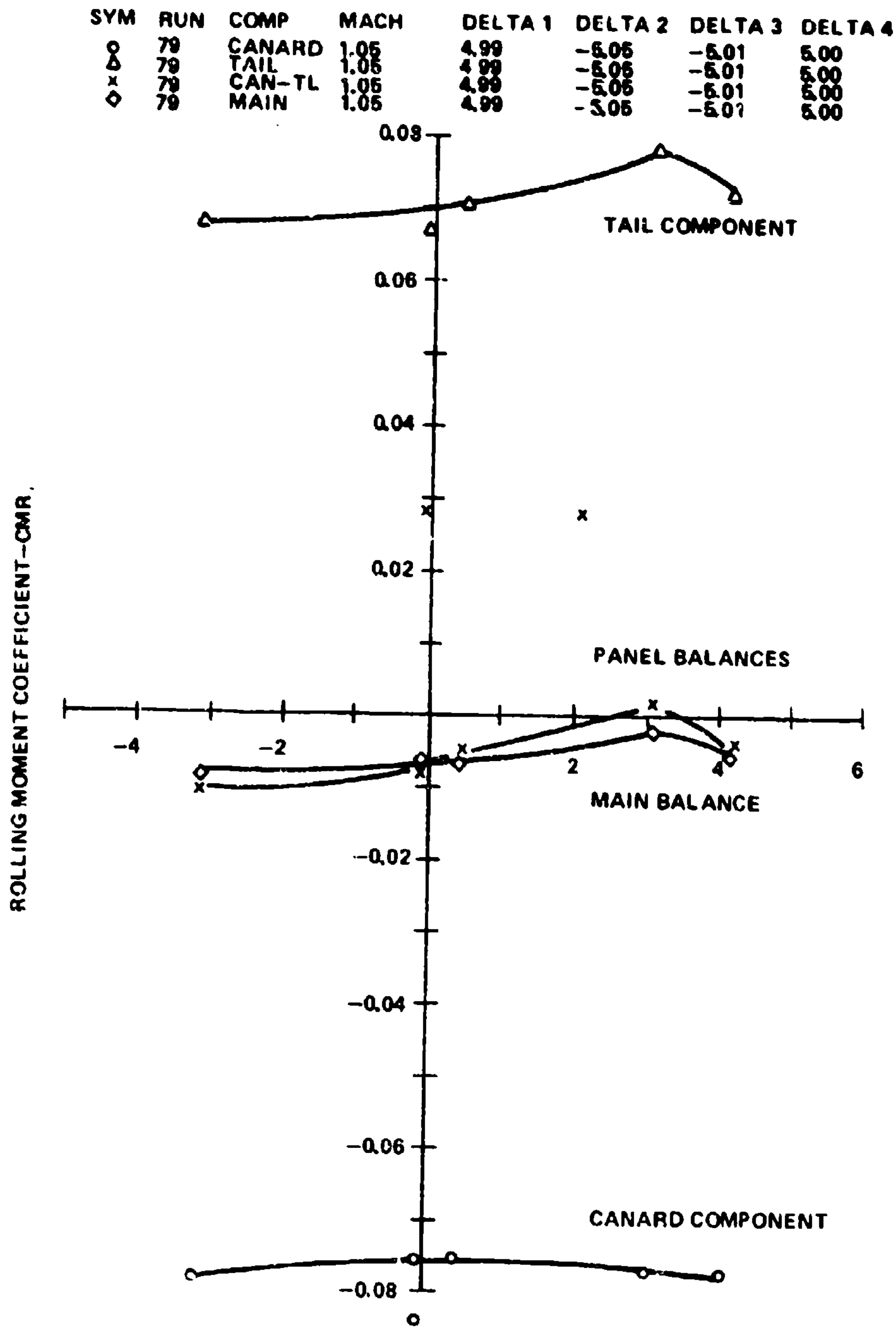

Figure 18. Component rolling moment coefficient, M_∞ = 1.05, aft canards, planar tail.

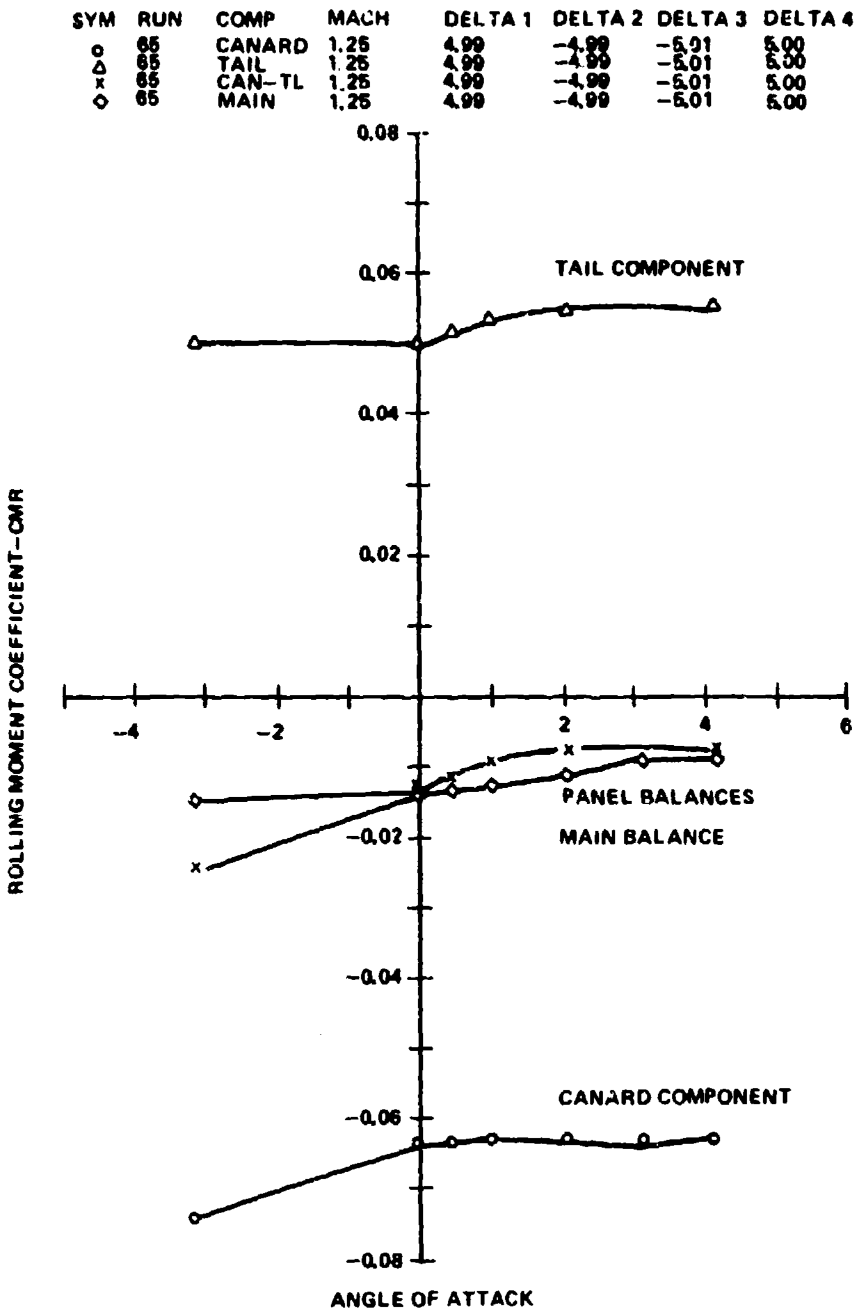

Figure 19. Component rolling moment coefficient, $M_{\infty} = 1.25$, aft canards, planar tail.

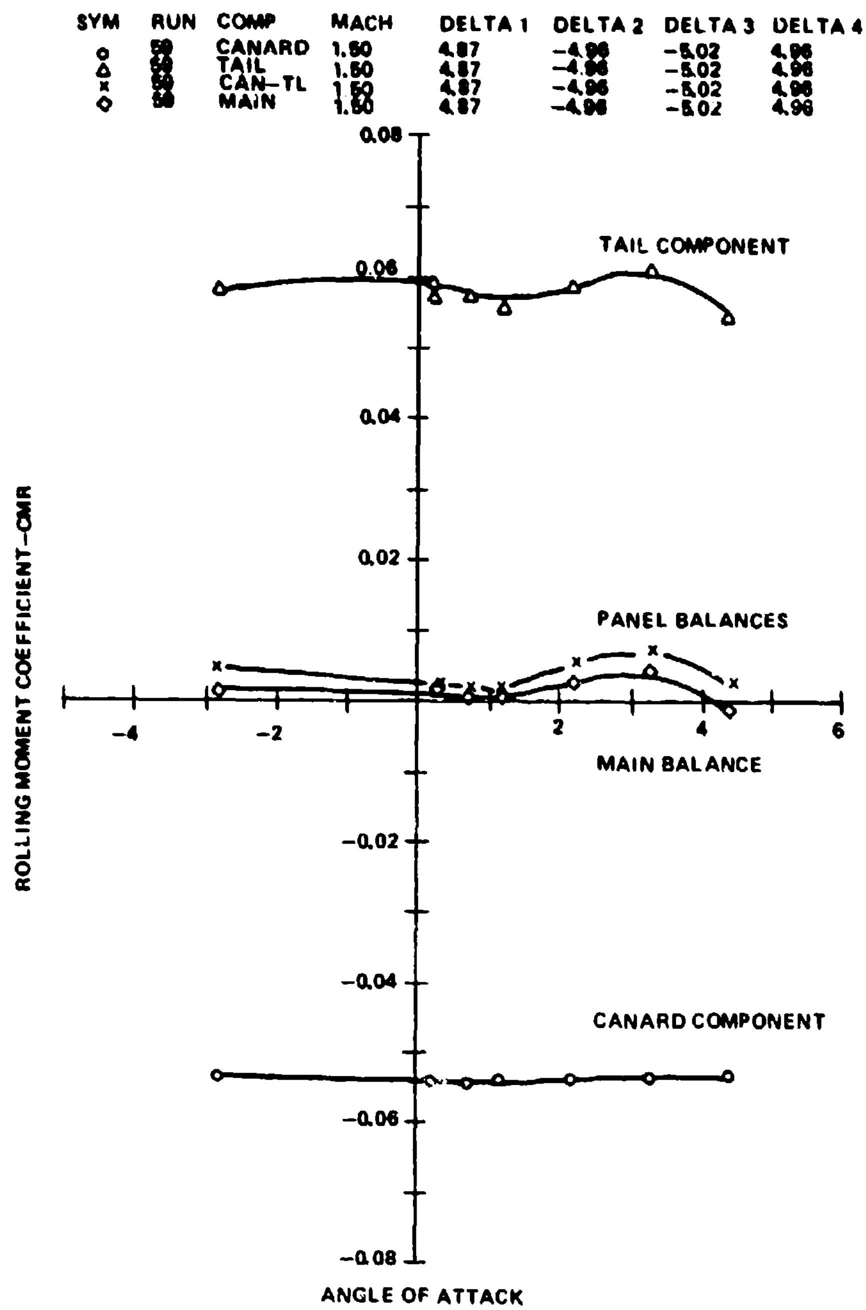

Figure 20. Component rolling moment coefficient, $M_\infty = 1.5$, aft canards, planar tail.

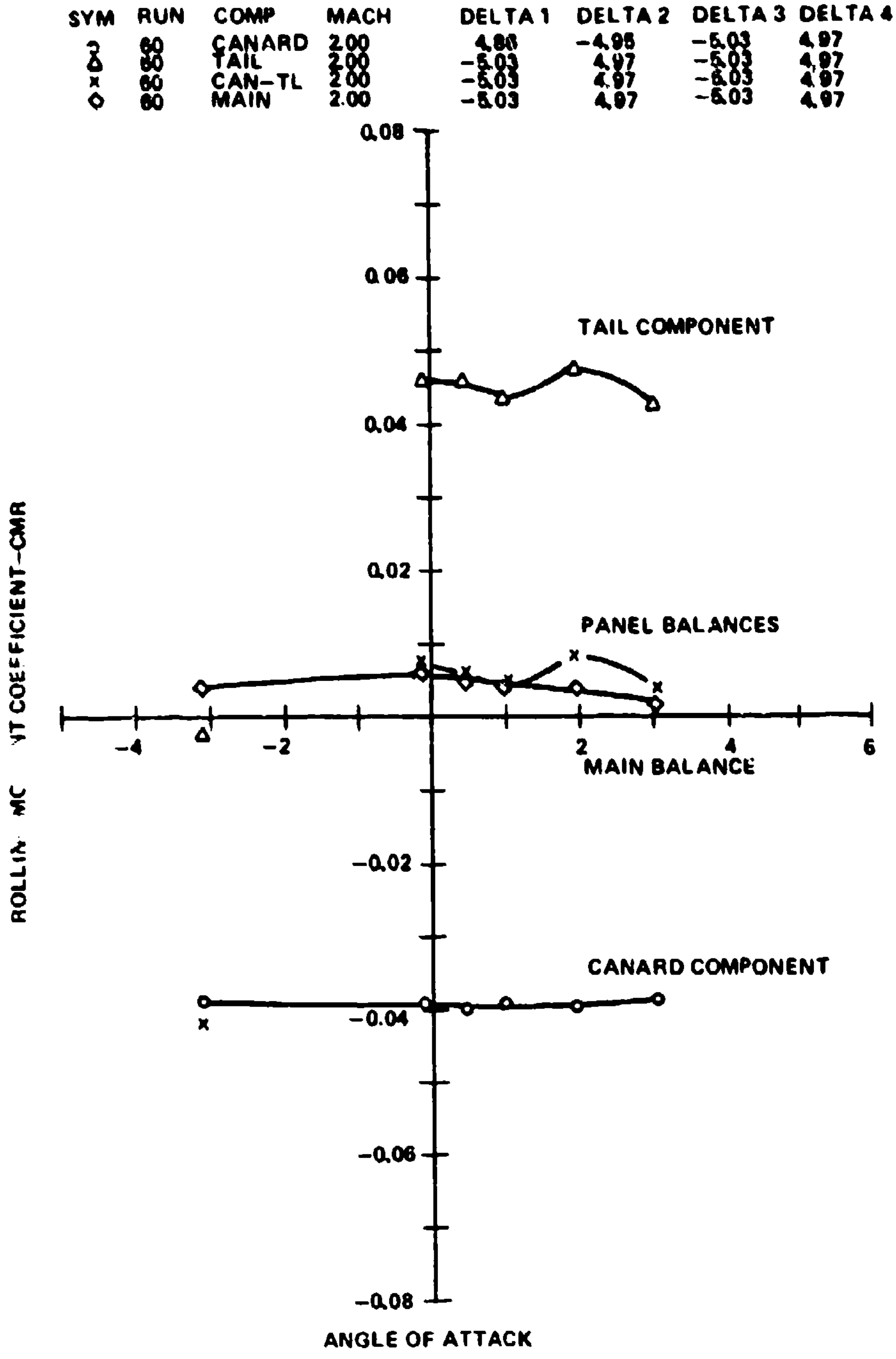

Figure 21. Component rolling moment coefficient, $M_\infty = 2.0$, aft canards, planar tail.

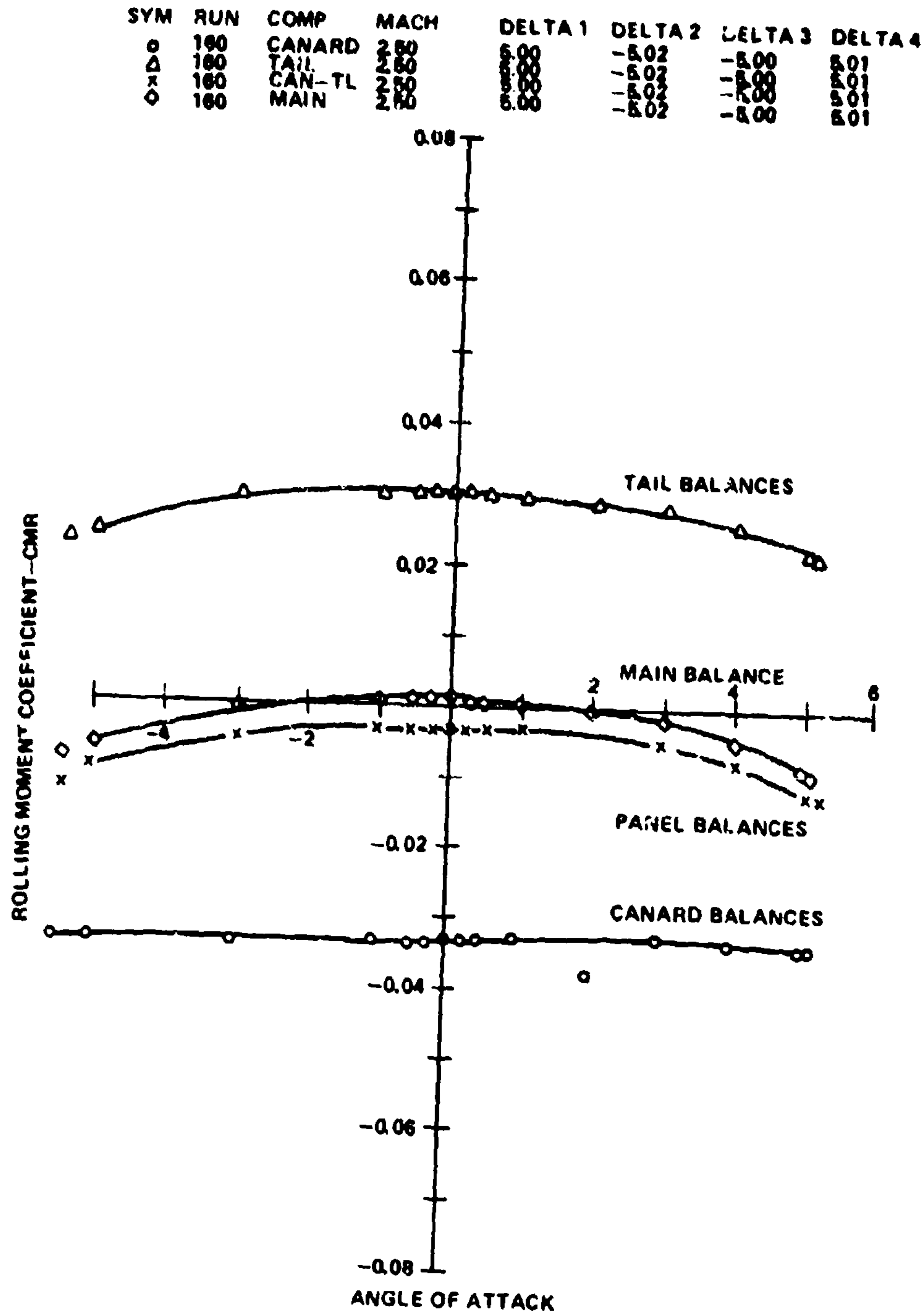

Figure 22. Component rolling moment coefficient, $M_\infty = 2.5$, aft canards, planar tail.

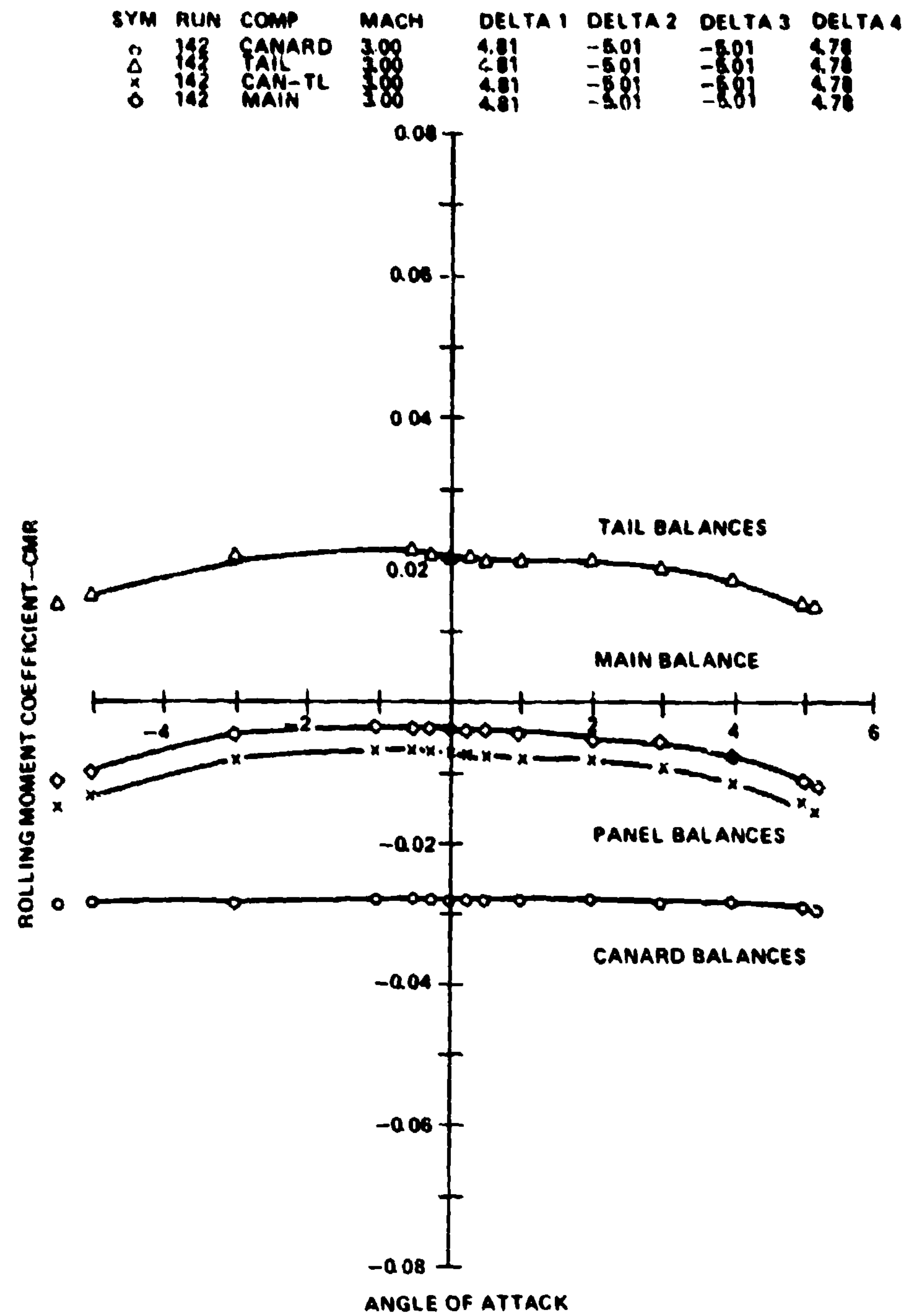

Figure 23. Component rolling moment coefficient, $M_\infty = 3.0$, aft canards, planar tail.

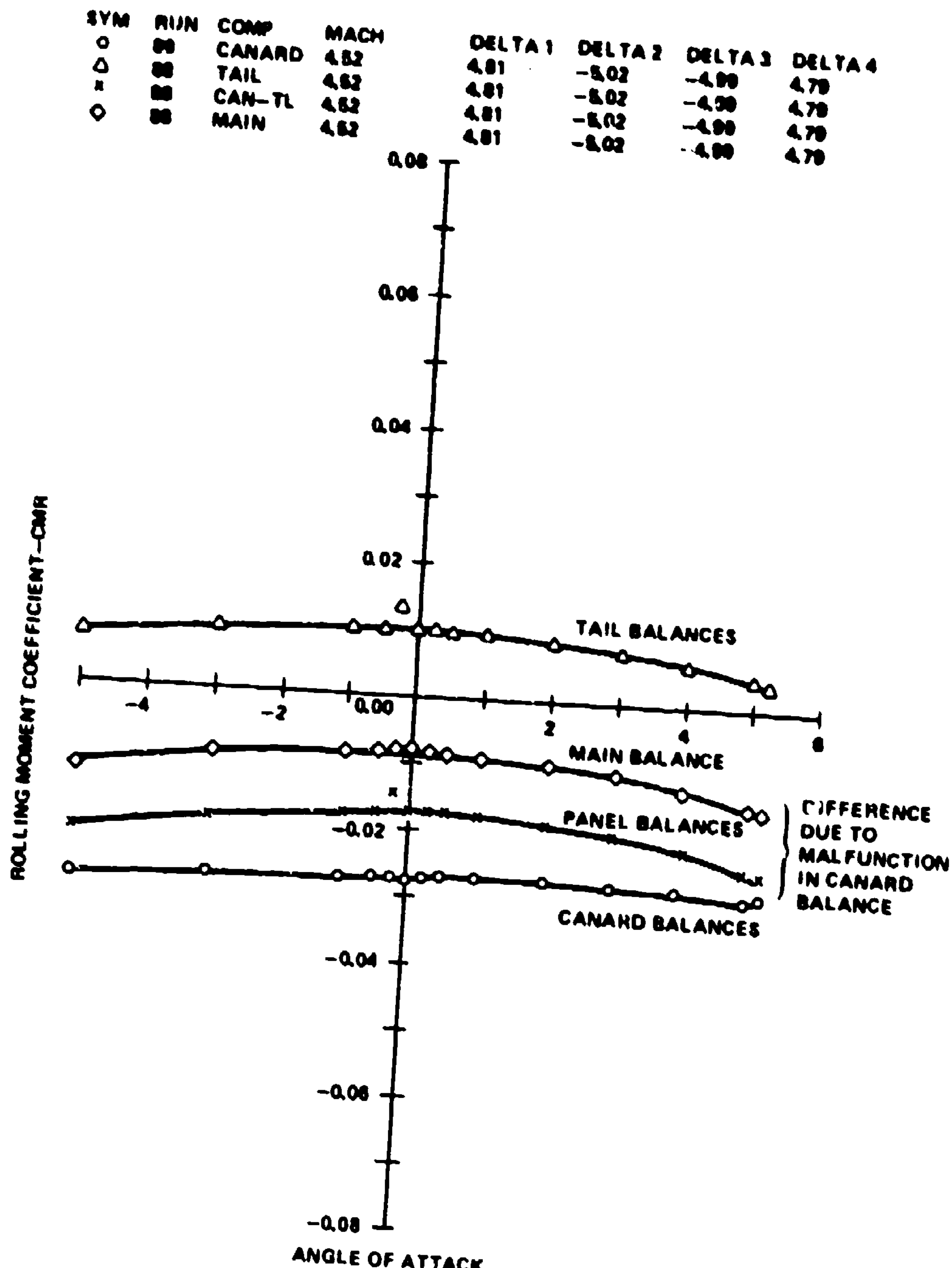

Figure 24. Component rolling moment coefficient, $M_\infty = 4.5$, aft canards, planar tail.

SYM	RUN	CONFIG	MACH	DELTA 1	DELTA 2	DELTA 3	DELTA 4
○	767		0.60	−3.00	3.00	3.00	−3.00
△	768	FORWARD	0.60	0.00	0.00	0.00	0.00
×	770		0.60	0.50	−0.50	−0.50	0.50
◇	772	CANARDS	0.60	1.00	−1.00	−1.00	1.00
□	774		0.60	2.00	−2.00	−2.00	2.00
○	776		0.60	5.00	−5.00	−5.00	5.00

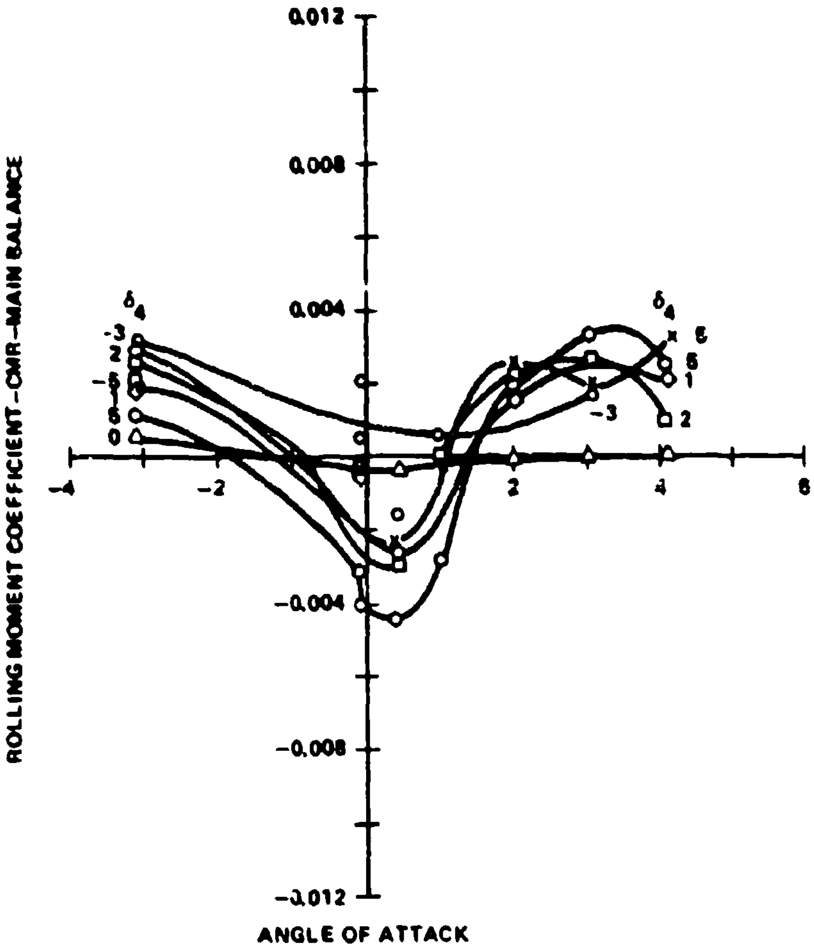

Figure 25. Total rolling moment coefficient, $M_\infty = 0.6$, forward canards, planar tail.

SYM	RUN	CONFIG	MACH	DELTA 1	DELTA 2	DELTA 3	DELTA 4
○	748		0.80	-3.00	3.00	3.00	-3.00
△	749	FORWARD	0.80	0.00	0.00	0.00	0.00
×	751		0.80	0.50	-0.50	-0.50	0.50
◇	753	CANARDS	0.80	1.00	-1.00	-1.00	1.00
□	755		0.80	2.00	-2.00	-2.00	2.00
○	757		0.80	5.00	-5.00	-5.00	5.00

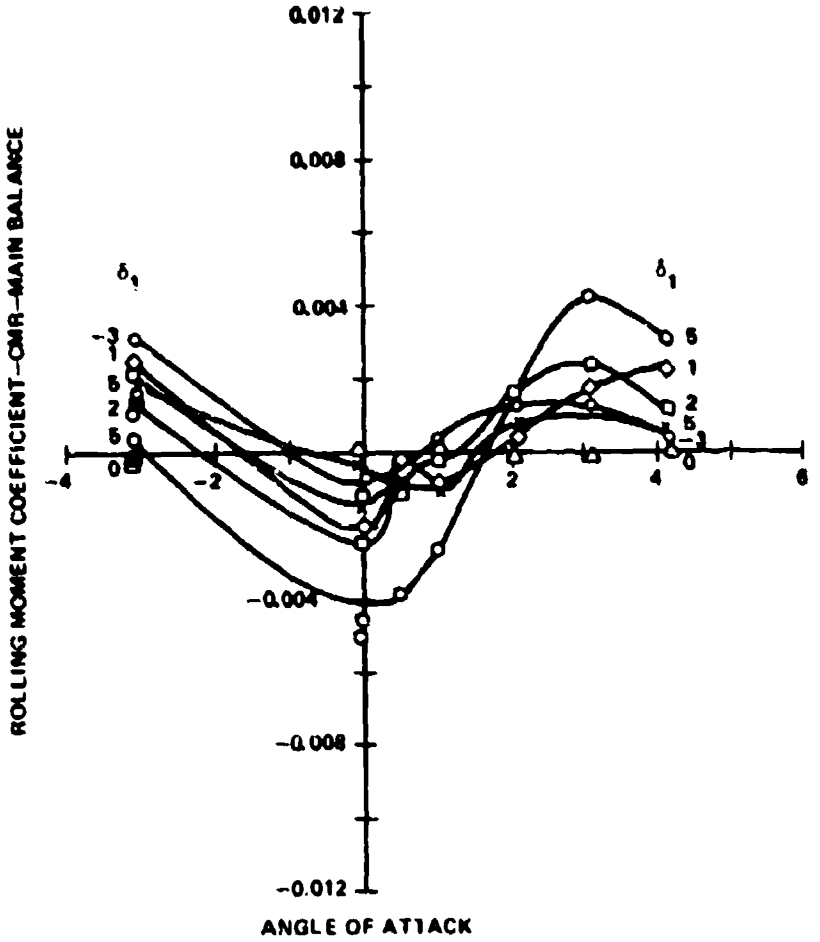

Figure 25 Total rolling moment coefficient, M_∞ = 0.8, forward canards, planar tail.

SYM	RUN	CONFIG	MACH	DELTA 1	DELTA 2	DELTA 3	DELTA 4
o	692		0.90	−3.00	3.00	3.00	−3.00
△	693	FORWARD	0.90	0.00	0.00	0.00	0.00
x	696		0.90	0.50	−0.50	−0.50	0.50
◇	697	CANARDS	0.90	1.00	−1.00	−1.00	1.00
□	699		0.90	2.00	−2.00	−2.00	2.00
o	701		0.90	5.00	−5.00	−5.00	5.00

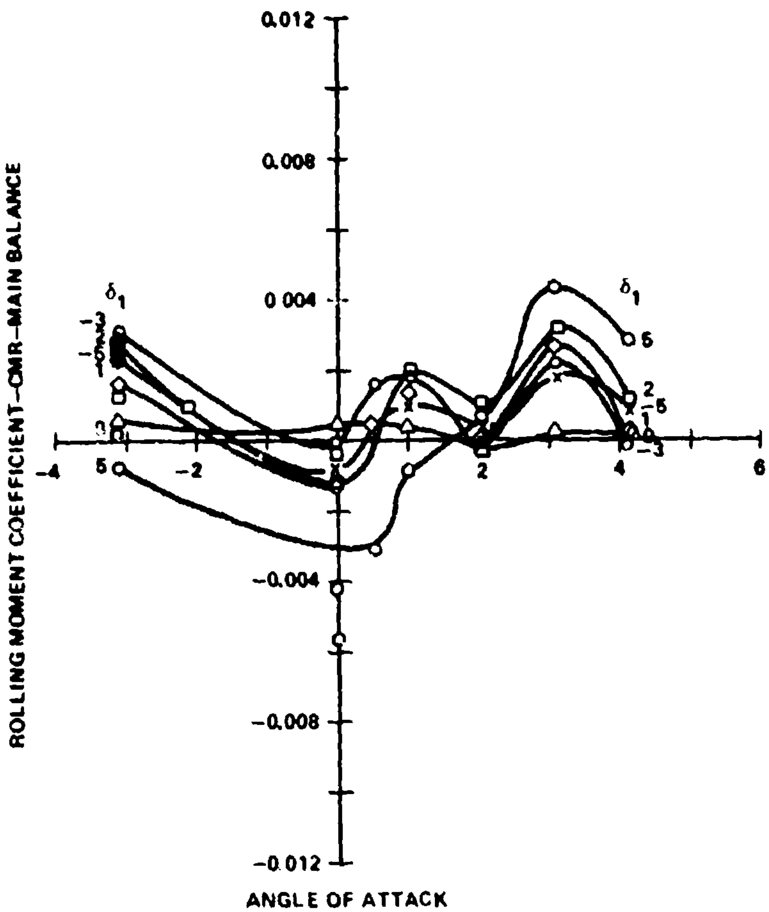

Figure 27 Total rolling moment coefficient, $M_\infty = 0.9$, forward canards, planar tail.

SYM	RUN	CONFIG	MACH	DELTA 1	DELTA 2	DELTA 3	DELTA 4
○	669		1.05	−3.00	3.00	3.00	−3.00
△	670	FORWARD	1.05	0.00	0.00	0.00	0.00
×	672	CANARDS	1.05	0.50	−0.50	−0.50	0.50
◇	674		1.05	1.00	−1.00	−1.00	1.00
□	676		1.05	2.00	−2.00	−2.00	2.00
○	678		1.05	5.00	−5.00	−5.00	5.00

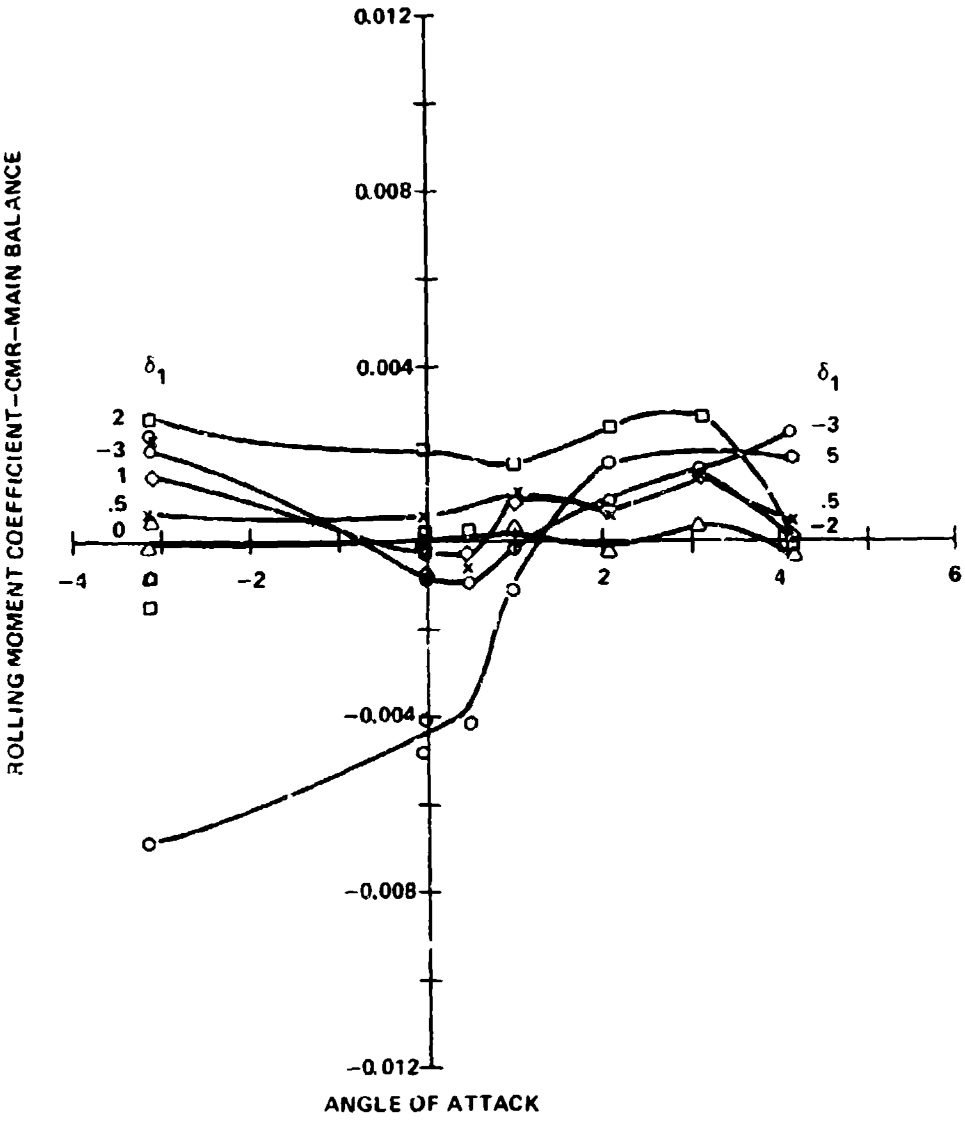

Figure 28. Total rolling moment coefficient, M_∞ = 1.05, forward canards, planar tail.

SYM	RUN	CONFIG	MACH	DELTA 1	DELTA 2	DELTA 3	DELTA 4
○	642	FORWARD CANARDS	1.25	−3.00	3.00	3.00	−3.00
△	643		1.25	0.00	0.00	0.00	0.00
×	645		1.25	0.50	−0.50	−0.50	0.50
◇	647		1.25	1.00	−1.00	−1.00	1.00
□	649		1.25	2.00	−2.00	−2.00	2.00
○	651		1.25	3.00	−5.00	−5.00	5.00

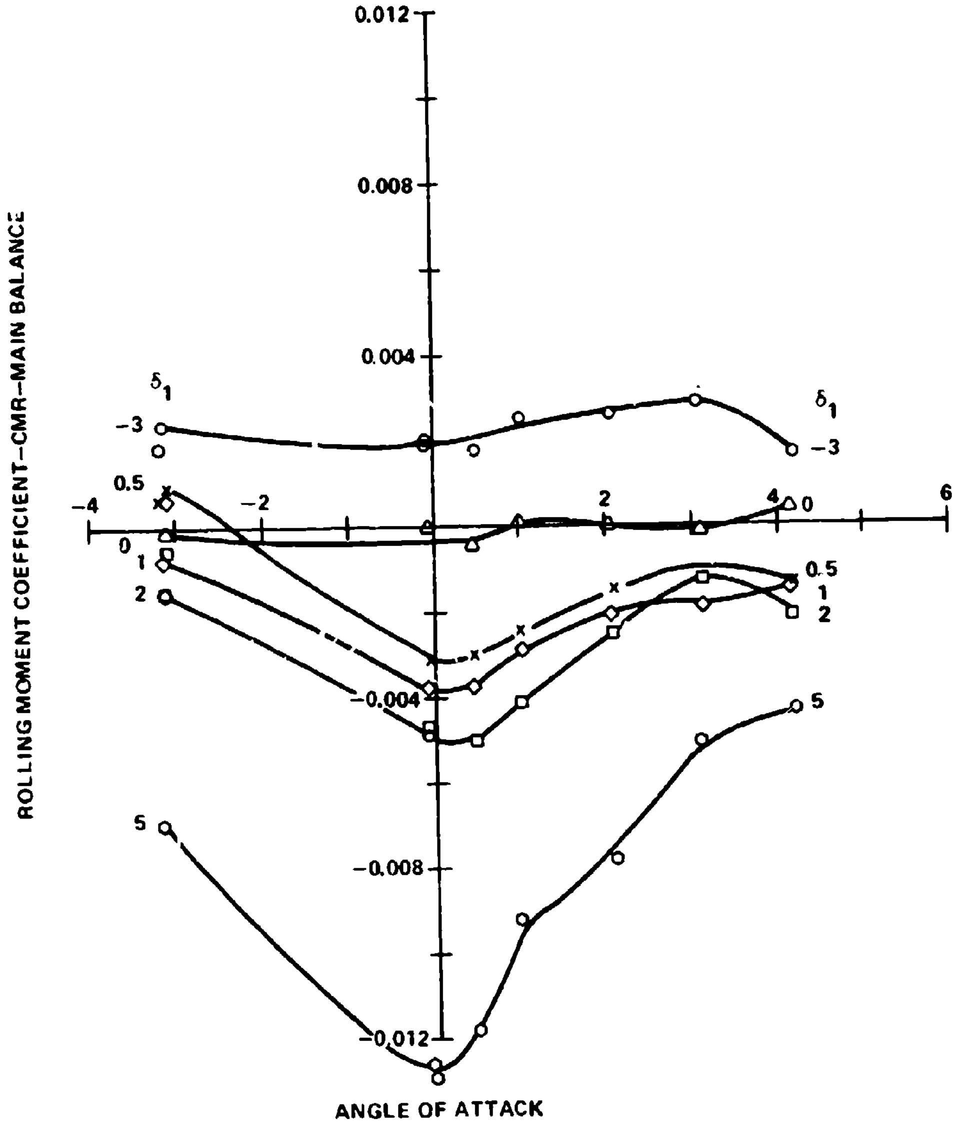

Figure 29. Total rolling moment coefficient, $M_\infty = 1.25$, forward canards, planar tail.

SYM	RUN	CONFIG	MACH	DELTA 1	DELTA 2	DELTA 3	DELTA 4
o	458	FORWARD	1.50	−3.03	3.01	3.04	−3.04
Δ	459		1.51	0.03	0.00	0.05	0.01
x	460	CANARDS	1.50	0.52	−0.51	−0.45	0.51
◇	461		1.50	0.96	−1.03	−0.94	0.99
□	462		1.50	1.97	−2.00	−1.92	1.98
O	463		1.50	4.38	−5.02	−4.95	5.04

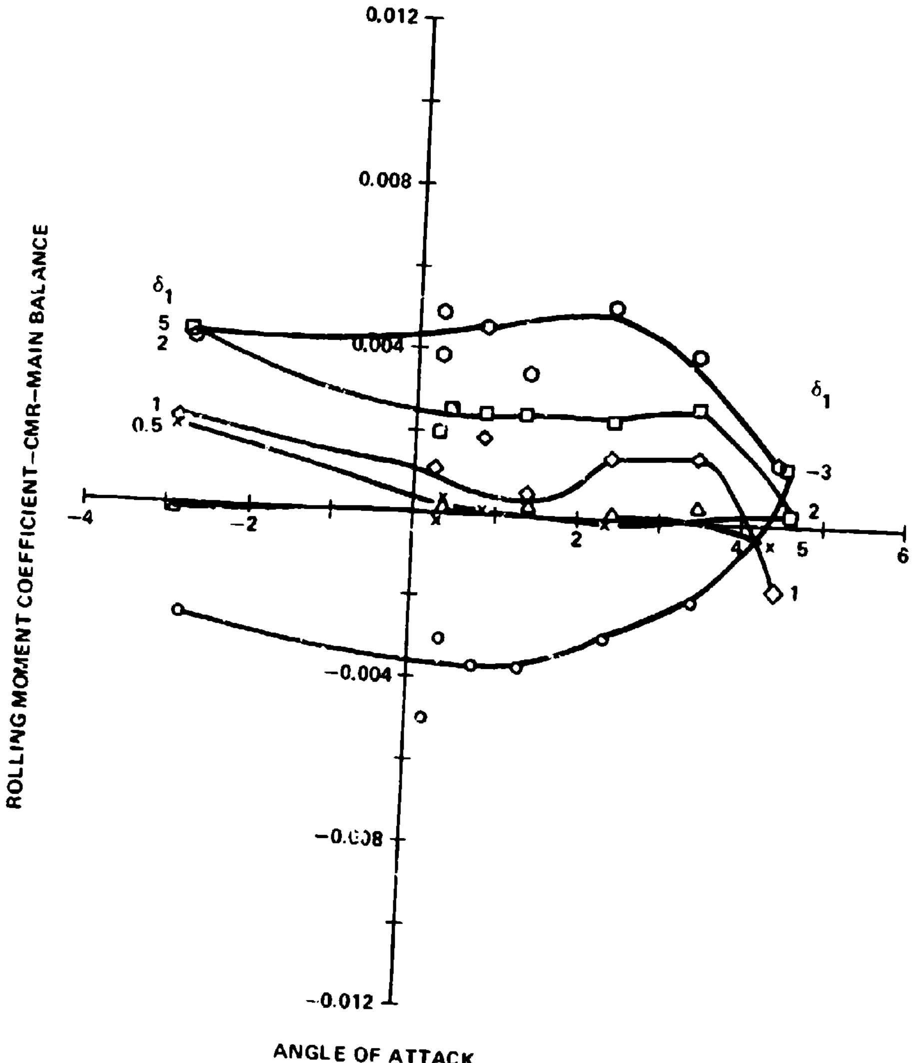

Figure 30. Total rolling moment coefficient, $M_\infty = 1.5$, forward canards, planar tail.

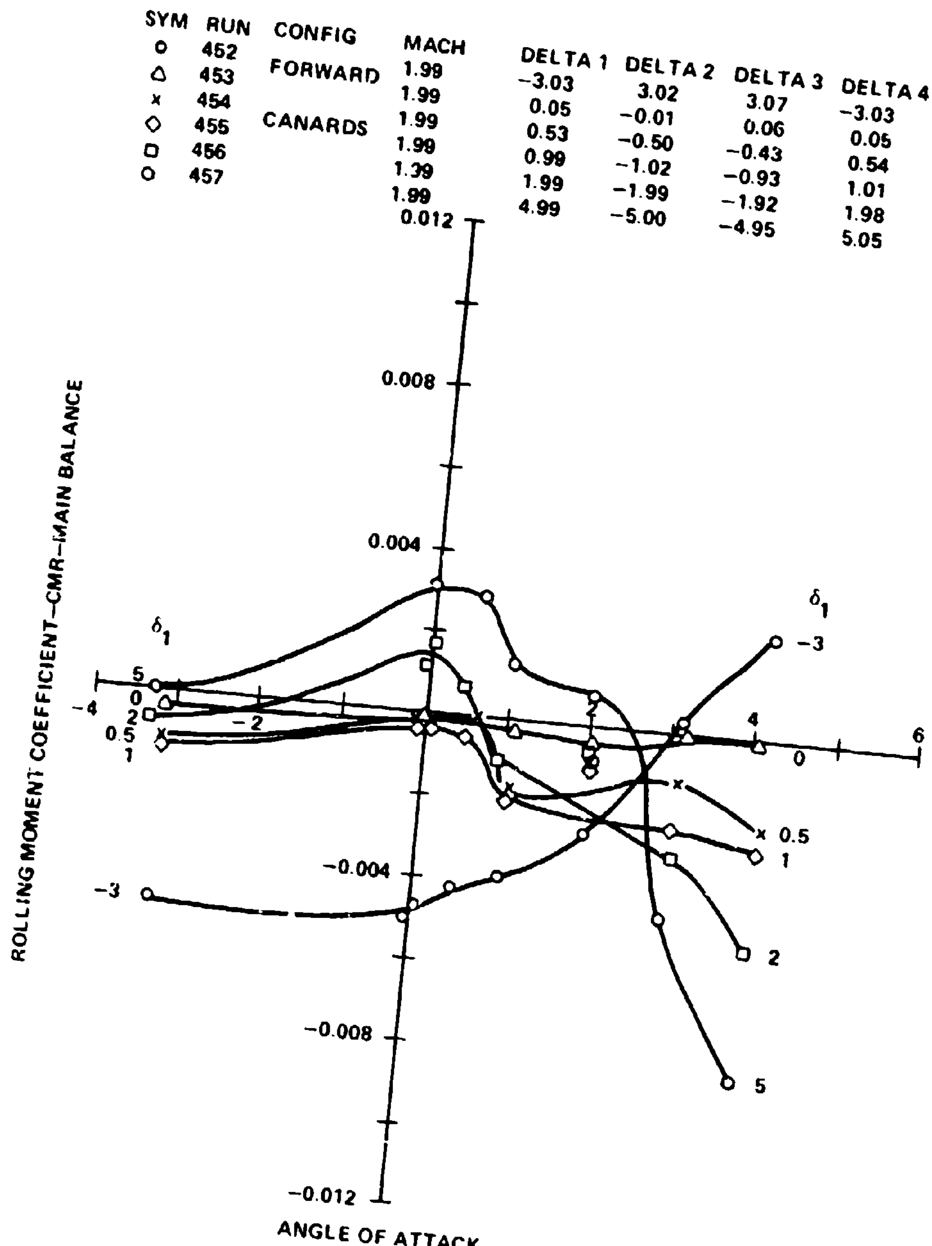

Figure 31. Total rolling moment coefficient, M_∞ = 2.0, forward canards, planar tail.

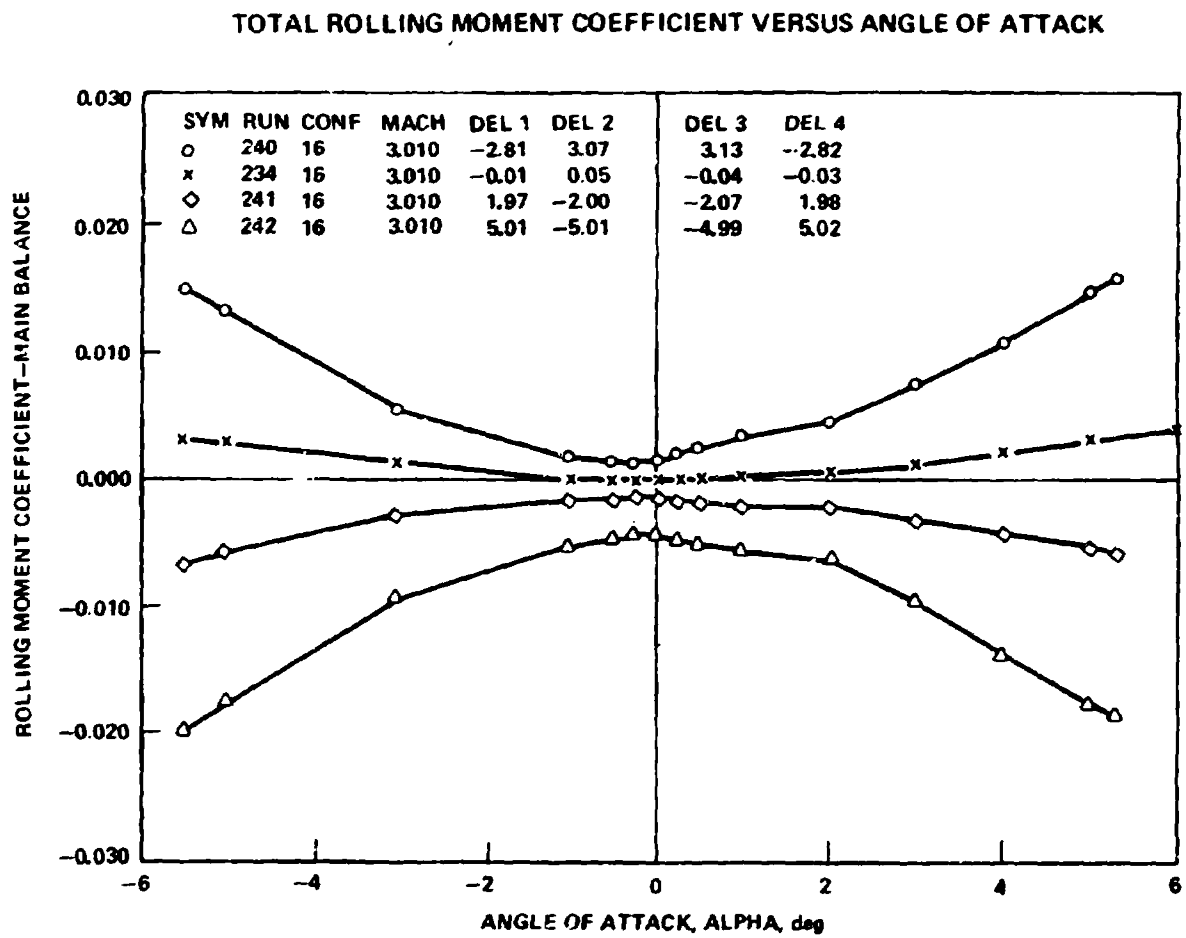

Figure 32. Total rolling moment coefficient, $M_\infty = 3.0$, forward canards, planar tail.

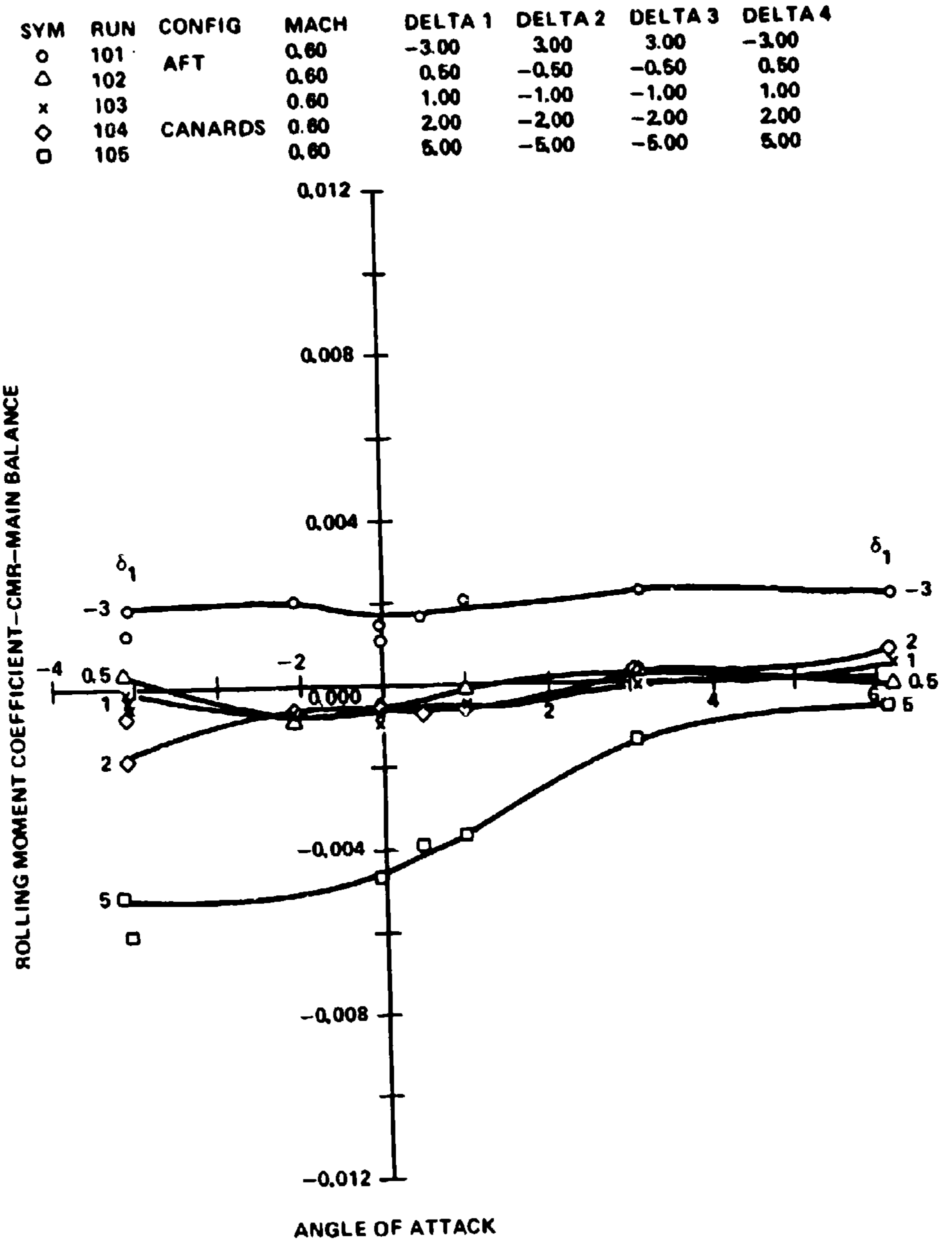

Figure 33. Total rolling moment coefficient, $M_\infty = 0.6$, aft canards, planar tail.

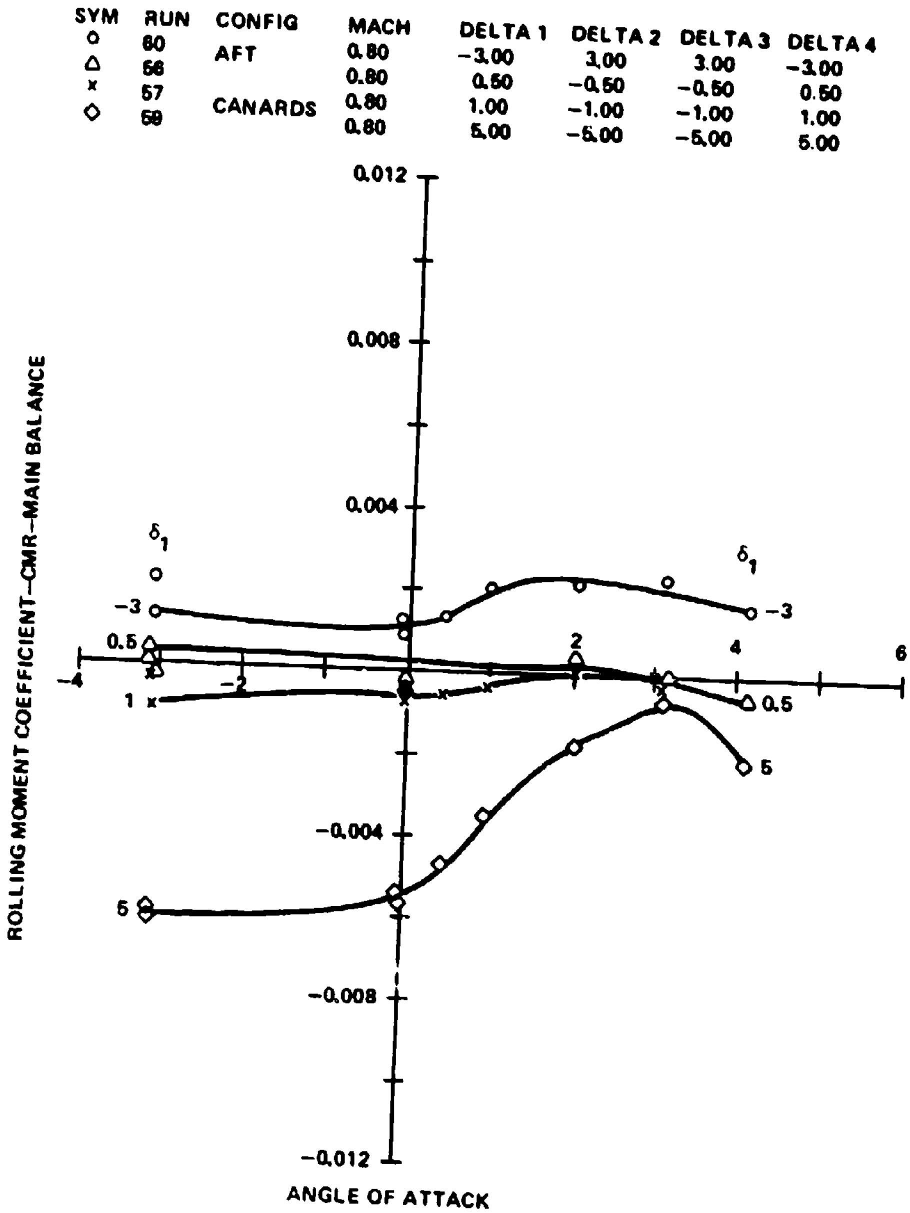

Figure 34. Total rolling moment coefficient, $M_\infty = 0.8$, aft canards, planar tail.

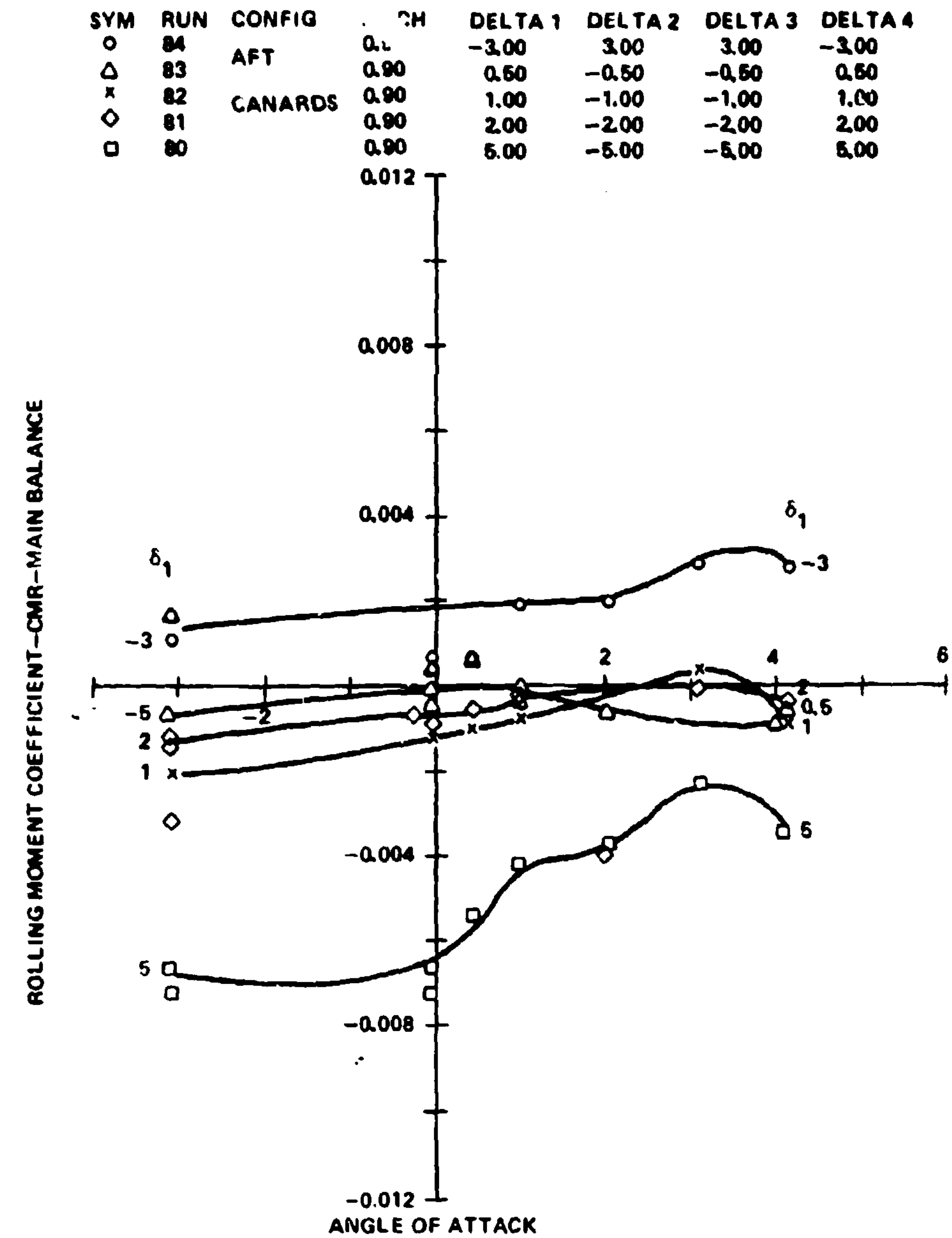

Figure 35. Total rolling moment coefficient, M_∞ = 0.9, aft canards, planar tail.

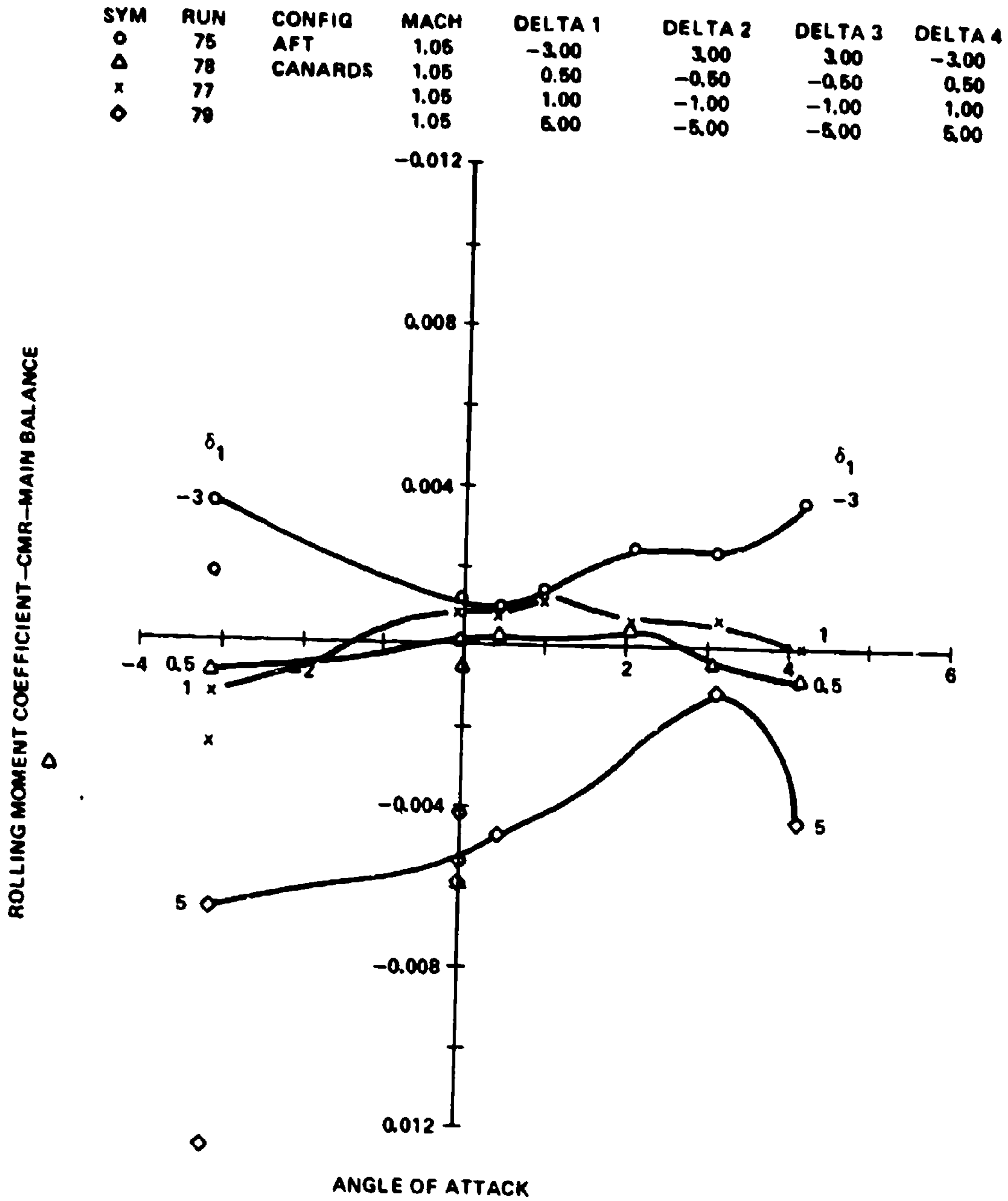

Figure 36. Total rolling moment coefficient, $M_\infty = 1.05$, aft canards, planar tail.

SYM	RUN	CONFIG	MACH	DELTA 1	DELTA 2	DELTA 3	DELTA 4
o	61	AFT	1.25	−3.00	3.00	3.00	−3.00
△	62	CANARDS	1.24	0.50	−0.50	−0.50	0.50
x	63		1.25	1.00	−1.00	−1.00	1.00
◇	64		1.25	2.00	−2.00	−2.00	2.00
□	65		1.25	5.00	−5.00	−5.00	5.00

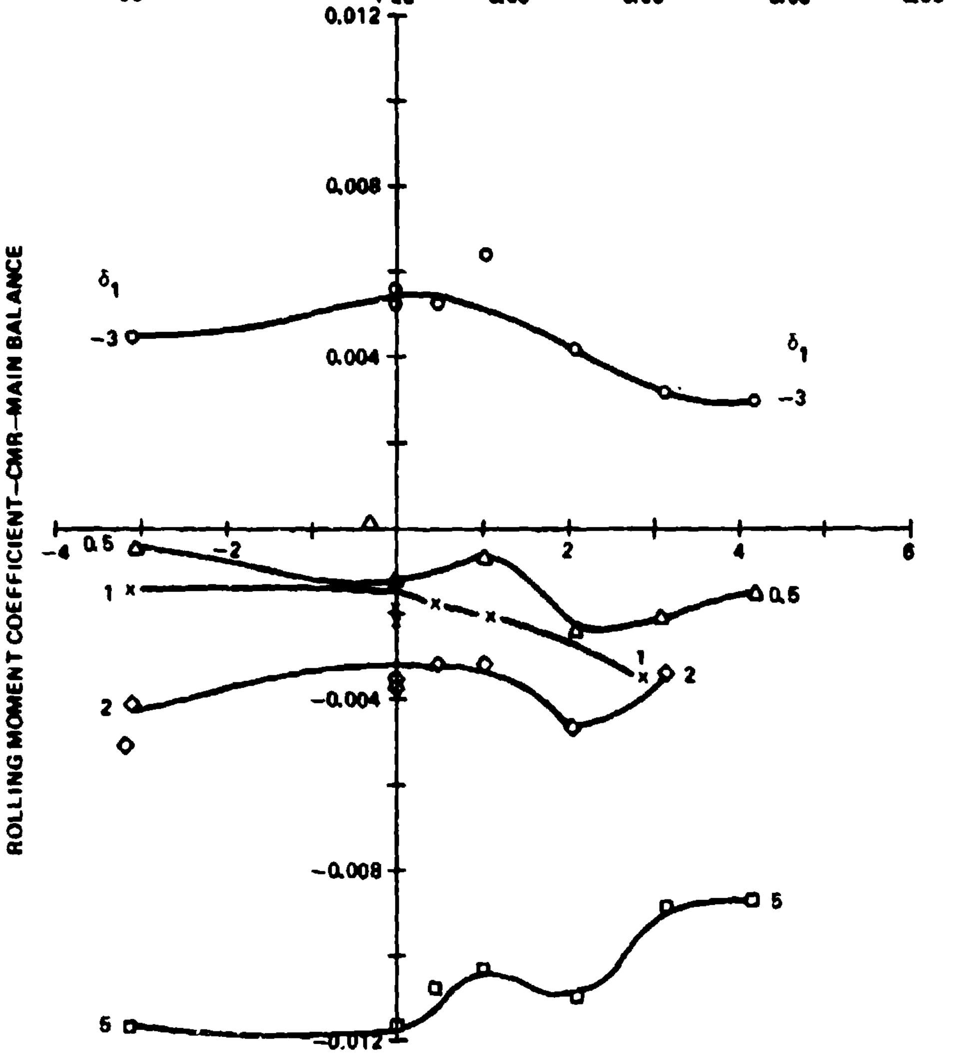

Figure 37. Total rolling moment coefficient, M_∞ = 1.25, aft canards, planar tail.

SYM	RUN	CONFIG	MACH	DELTA 1	DELTA 2	DELTA 3	DELTA 4
○	49	AFT	1.50	−3.08	2.99	2.99	−3.11
△	51	CANARDS	1.50	−0.05	−0.02	−0.05	−0.07
×	53		1.50	0.43	−0.47	−0.40	0.43
◇	55		1.50	0.91	−0.93	−1.01	0.93
□	57		1.50	1.93	−2.00	−1.99	1.94
○	59		1.50	4.87	−4.96	−5.02	4.96

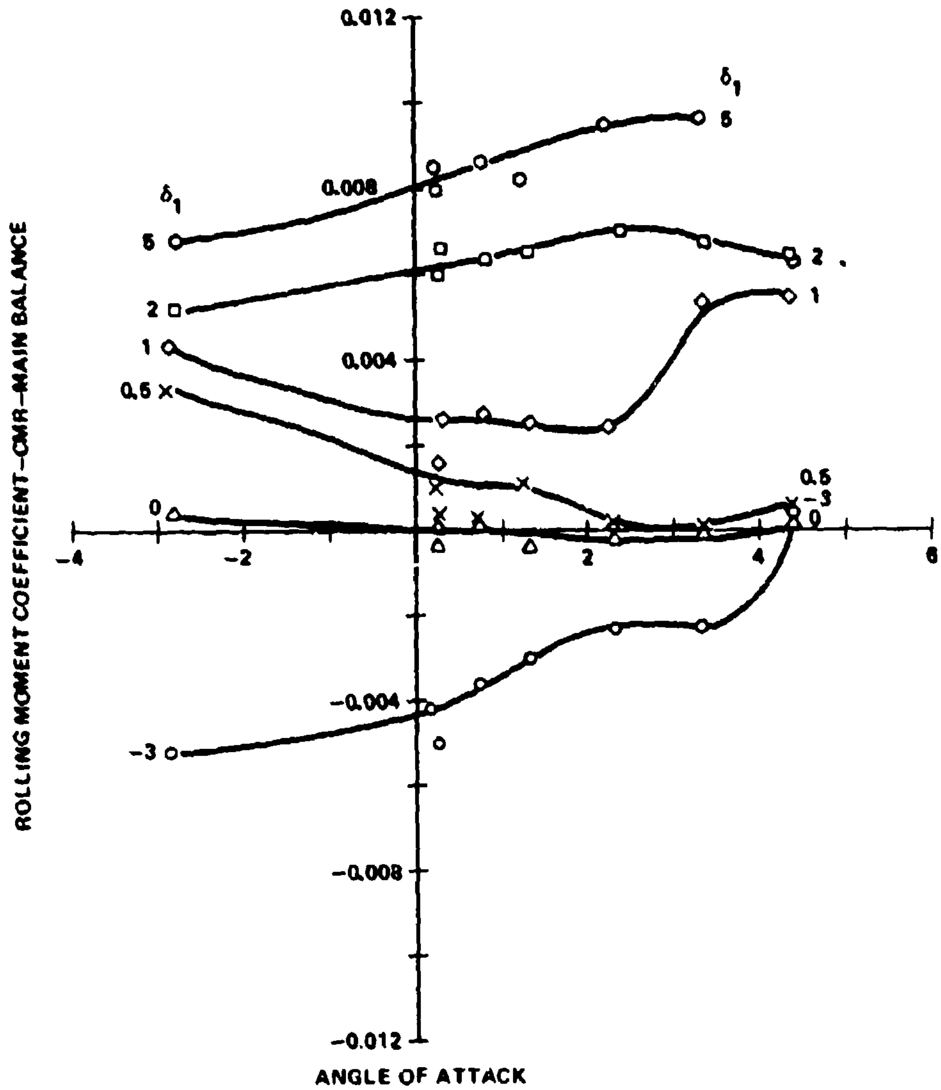

Figure 38. Total rolling moment coefficient, M_∞ = 1.5, aft canards, planar tail.

SYM	RUN	CONFIG	MACH	DELTA 1	DELTA 2	DELTA 3	DELTA 4
○	50		1.99	−3.06	2.99	2.98	−3.11
△	52	AFT	2.00	−0.04	−0.02	−0.06	−0.07
×	54		2.00	0.43	−0.48	−0.48	0.44
◇	56	CANARDS	1.99	0.93	−0.93	−1.01	0.93
□	58		1.99	1.93	−2.00	−1.96	1.96
○	60		2.00	4.06	−4.96	−5.03	4.97

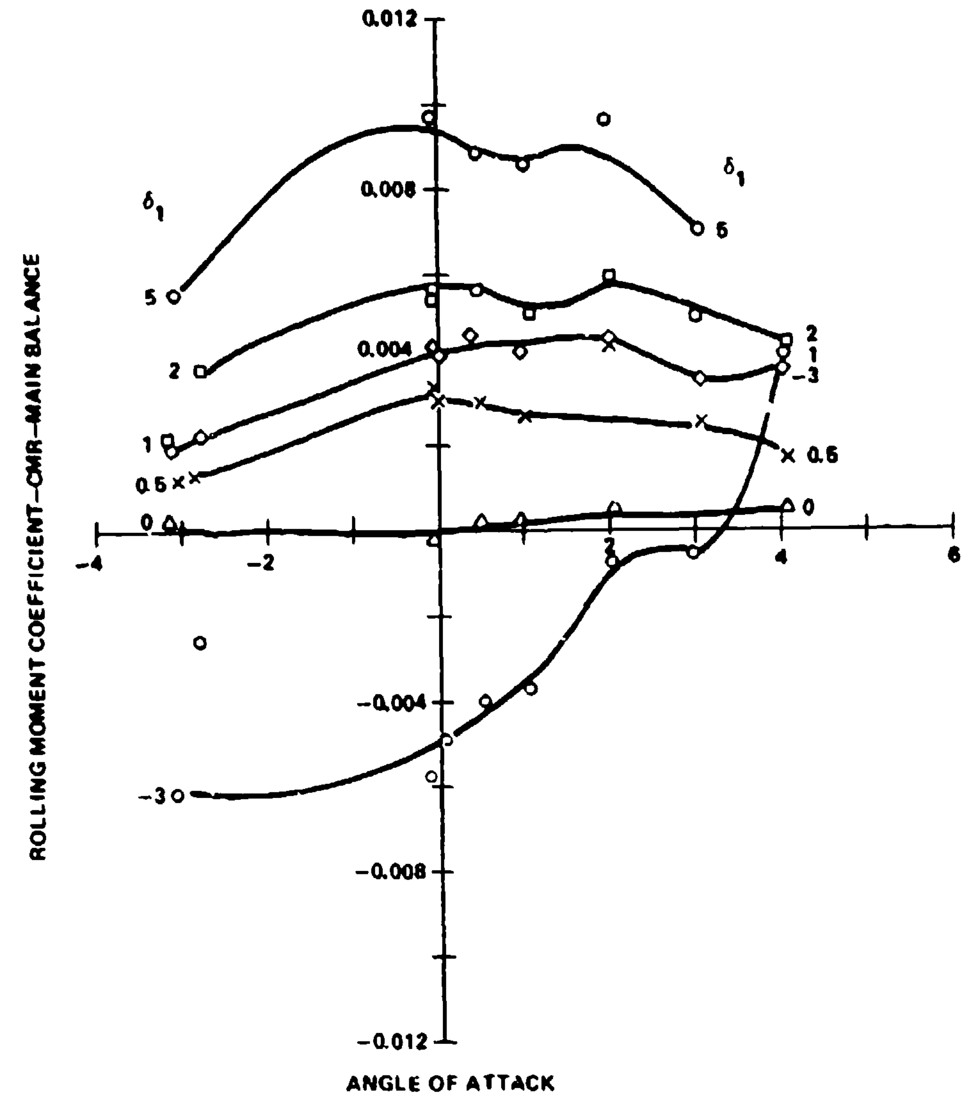

Figure 39. Total rolling moment coefficient, M_∞ = 2.0, aft canards, planar tail.

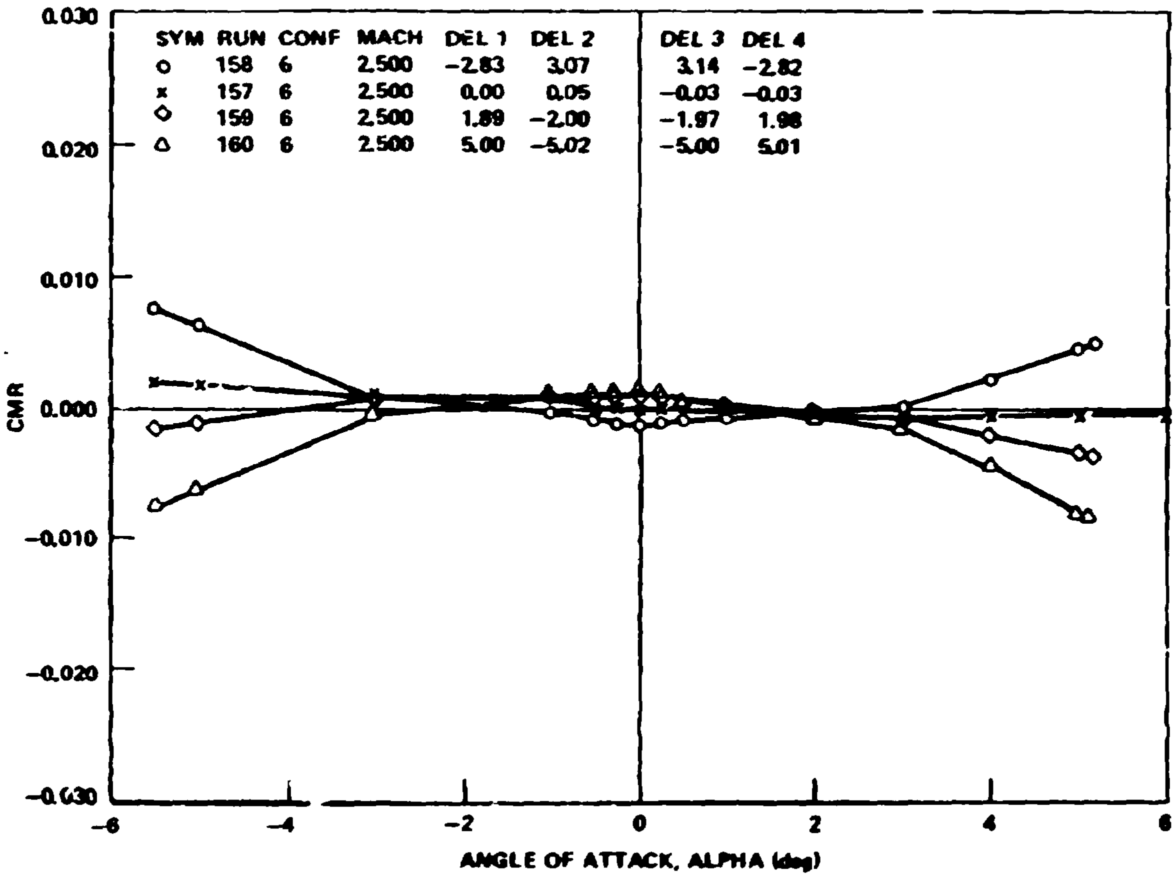

Figure 40. Total rolling moment coefficient versus angle of attack, aft canards, planar tail, M_∞ = 2.5.

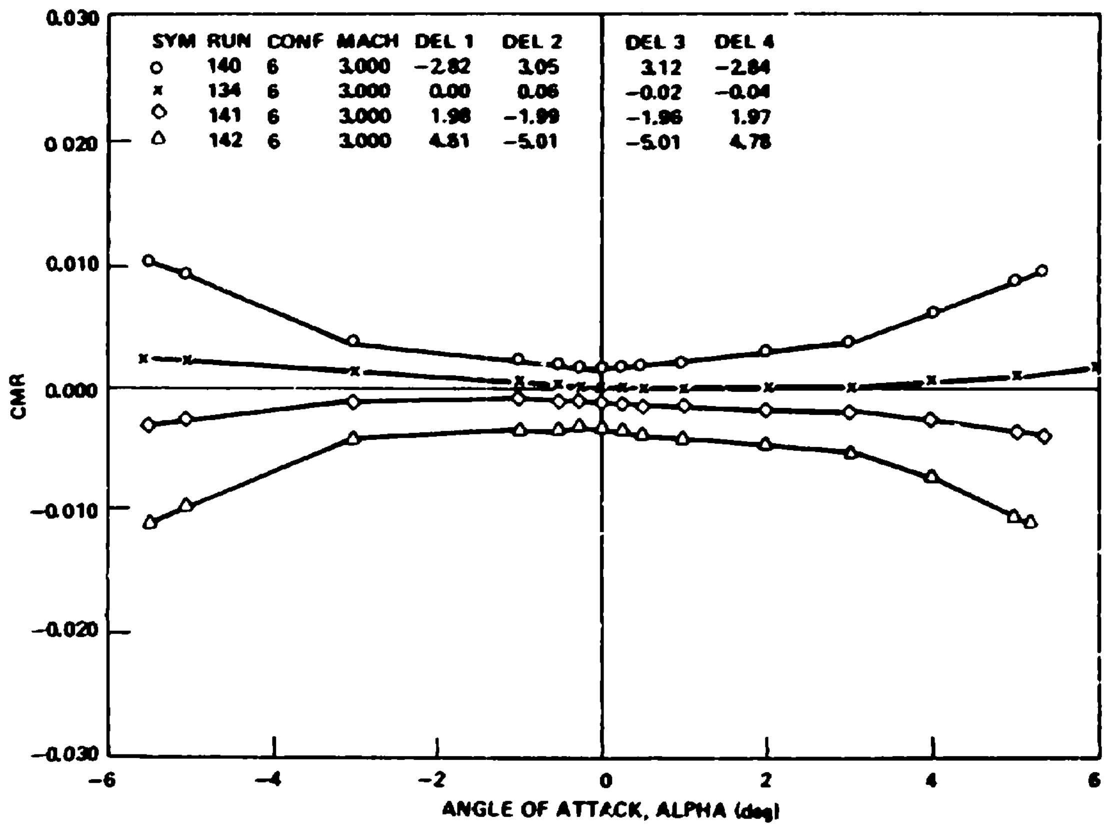

Figure 41. Total rolling moment coefficient versus angle of attack, aft canards, planar tail, $M_\infty = 3.0$.

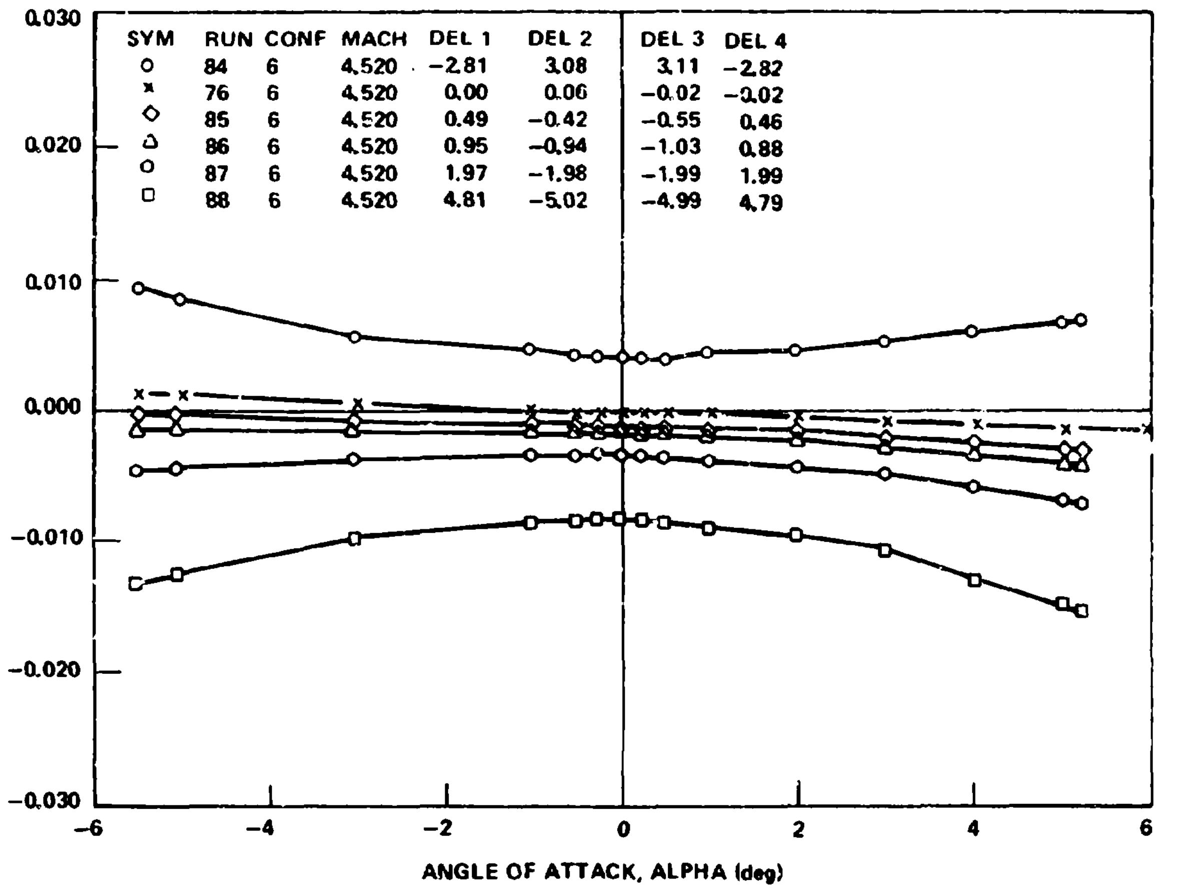

Figure 42. Total rolling moment coefficient versus angle of attack, aft canards, planar tail (runs 76 and 84 through 88).

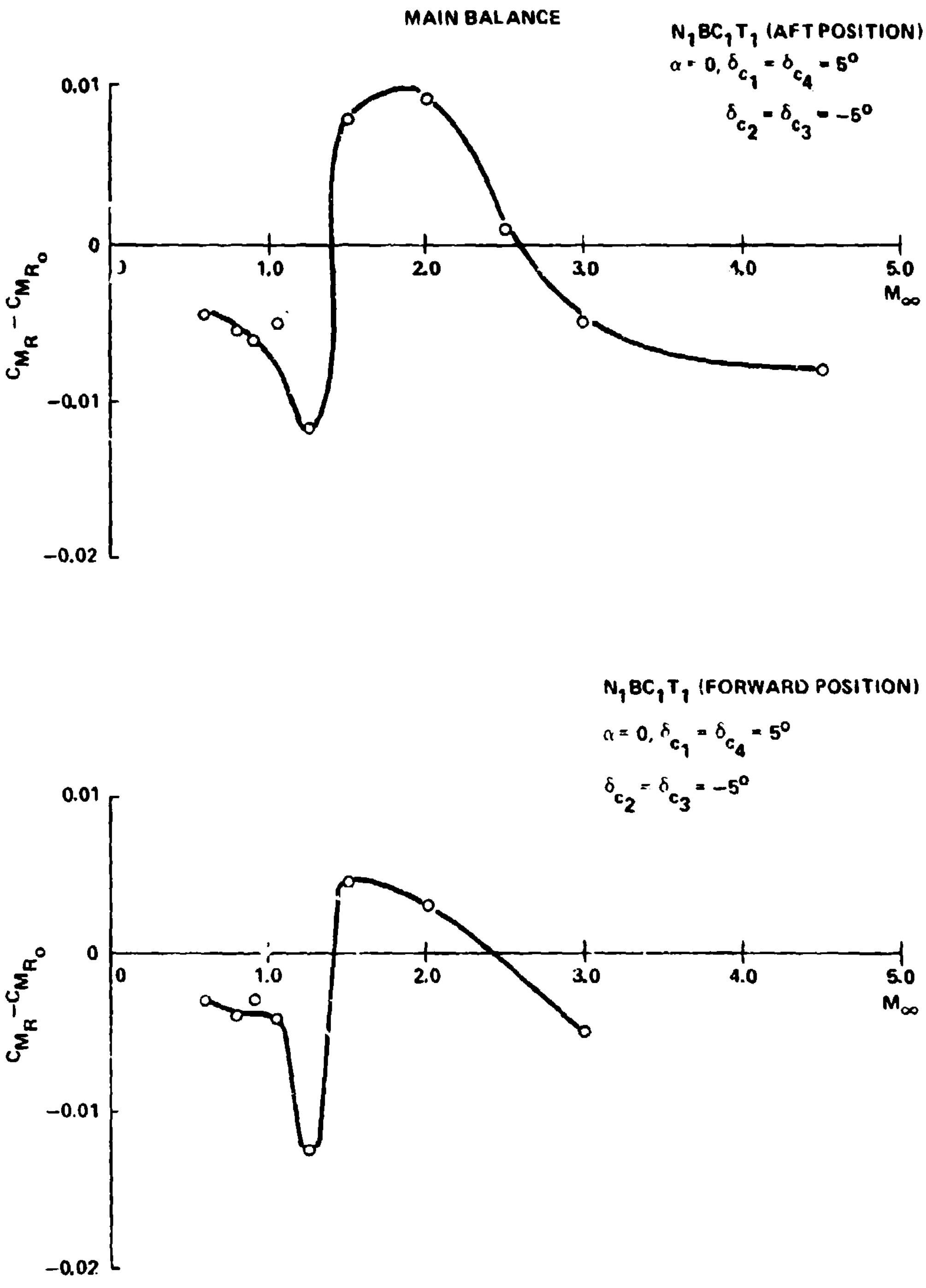

Figure 43. Effect of Mach number on rolling moment coefficients, $\alpha = 0$, $\delta = \pm 5°$.

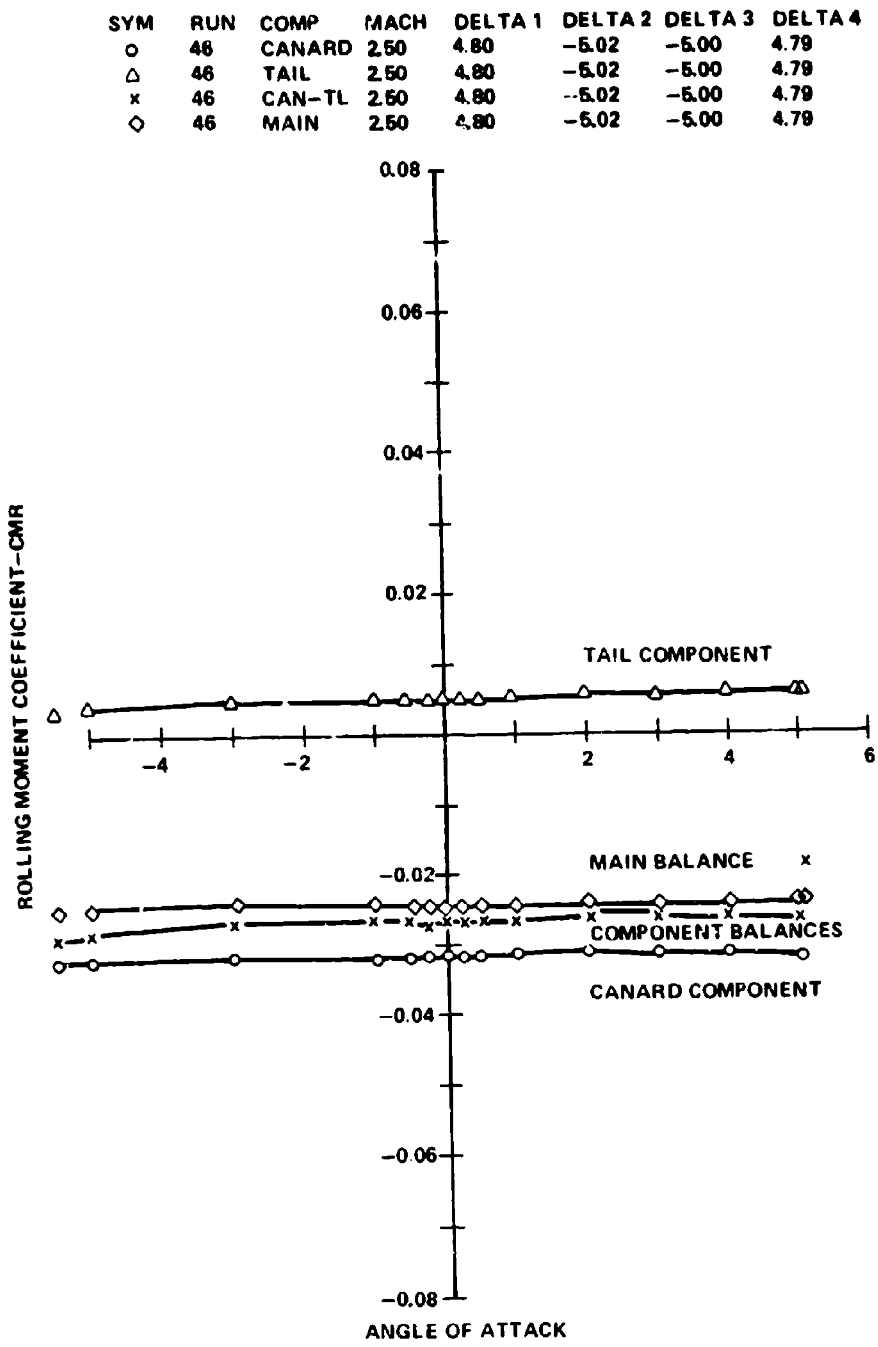

Figure 44. Component rolling moment coefficient, $M_\infty = 2.5$, aft canards, ring tail.

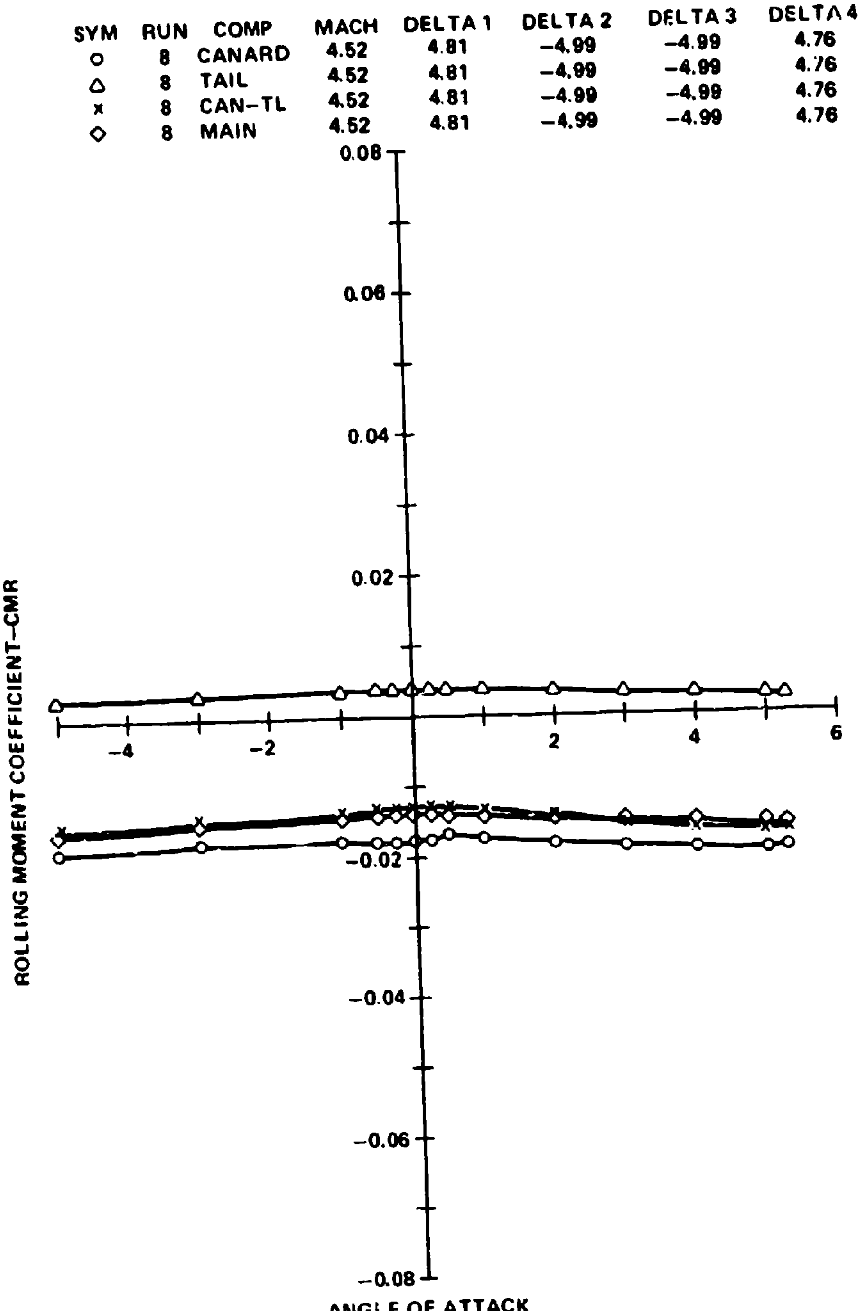

Figure 45. Component rolling moment coefficient, $M_\infty = 4.5$, aft canards, ring tail.

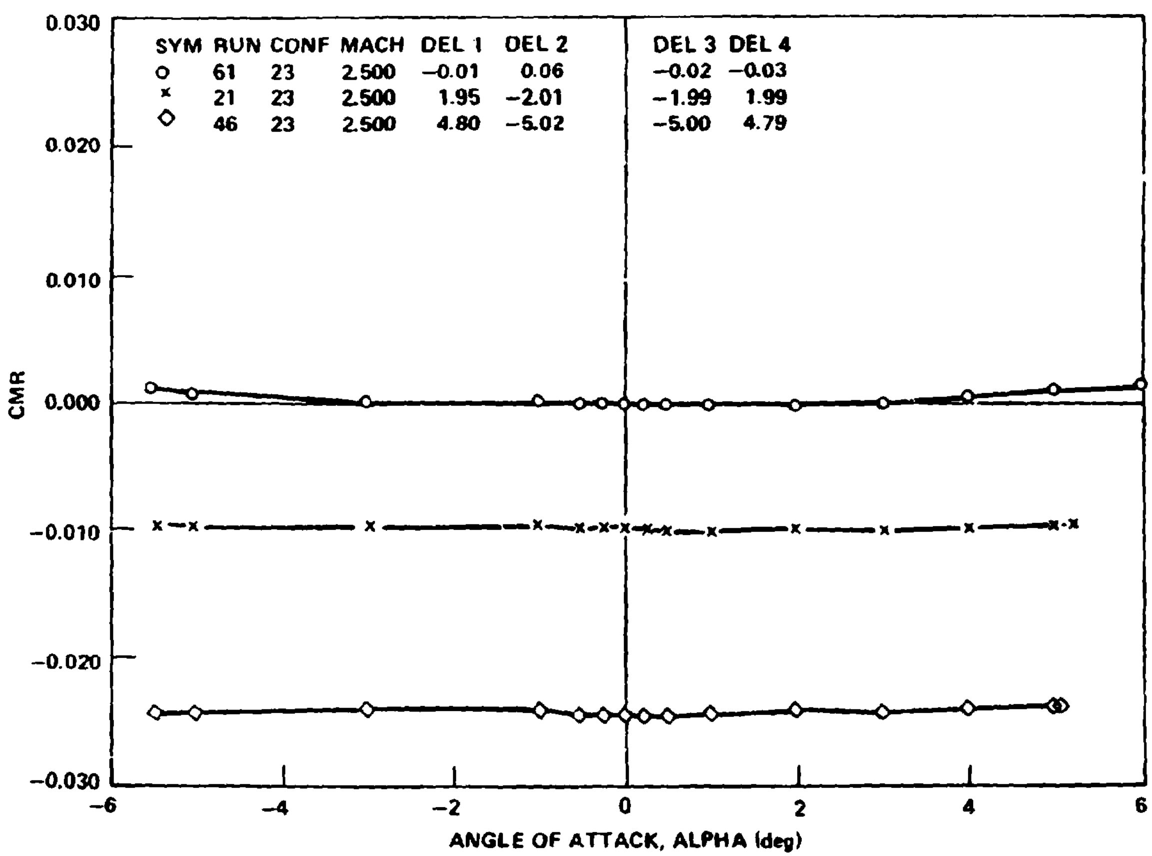

Figure 46. Total rolling moment coefficient versus angle of attack, $M_\infty = 2.5$, aft canard, ring tail.

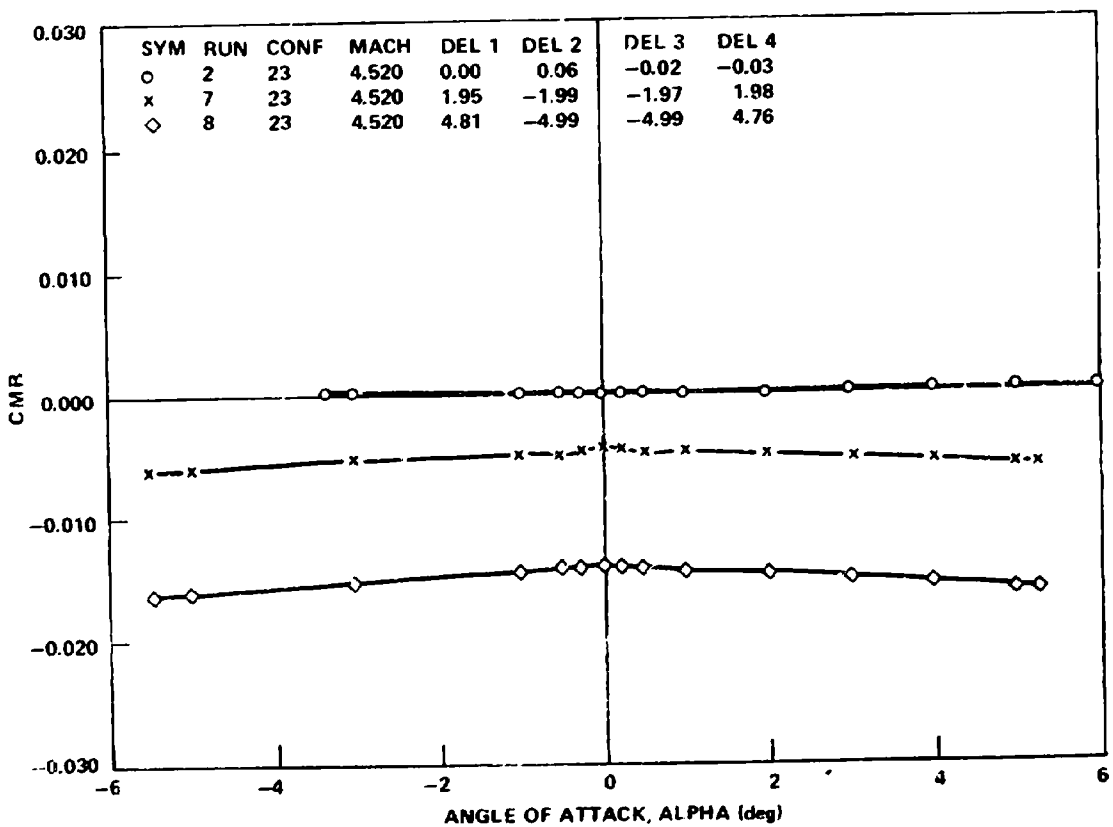

Figure 47. Total rolling moment coefficient versus angle of attack, $M_\infty = 4.5$, aft canard, ring tail.

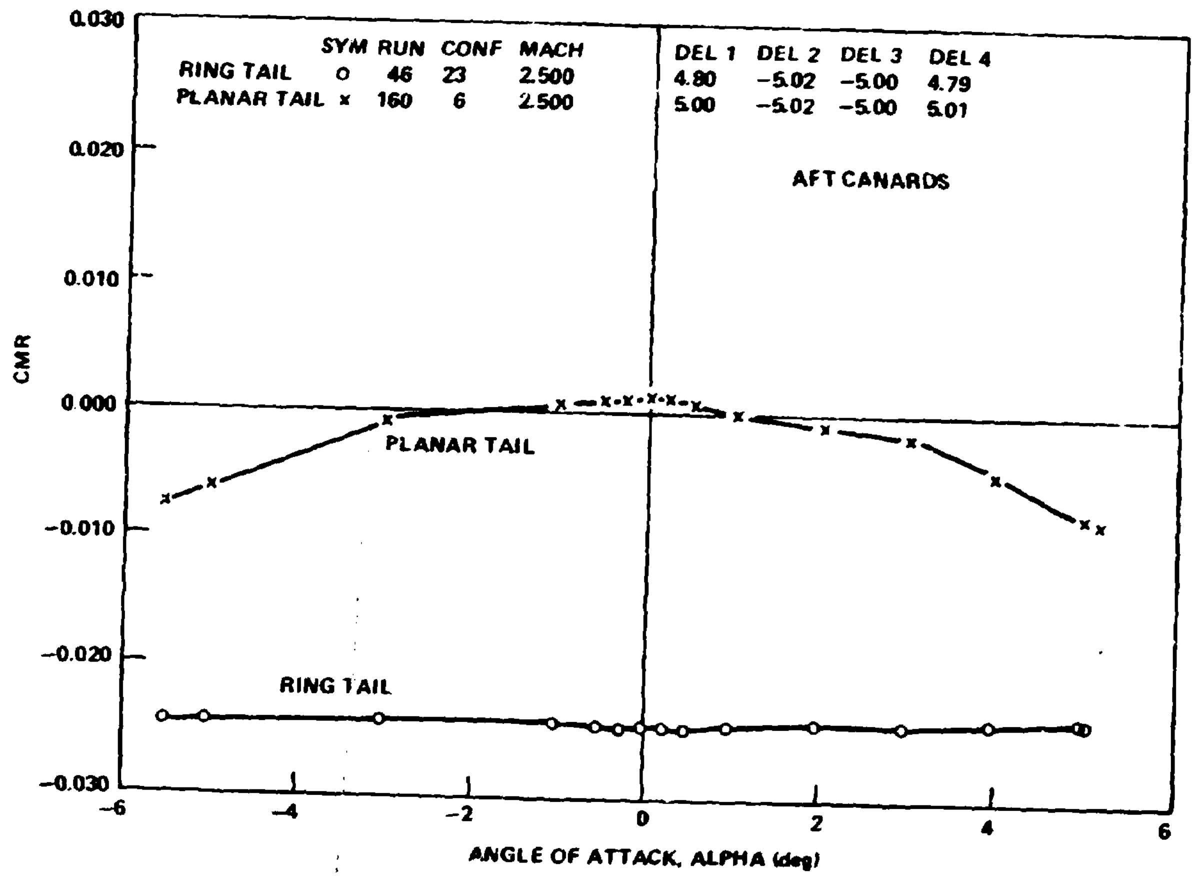

Figure 48. Total rolling moment coefficient versus angle of attack, $M_\infty = 2.5$, planar tail, ring tail.

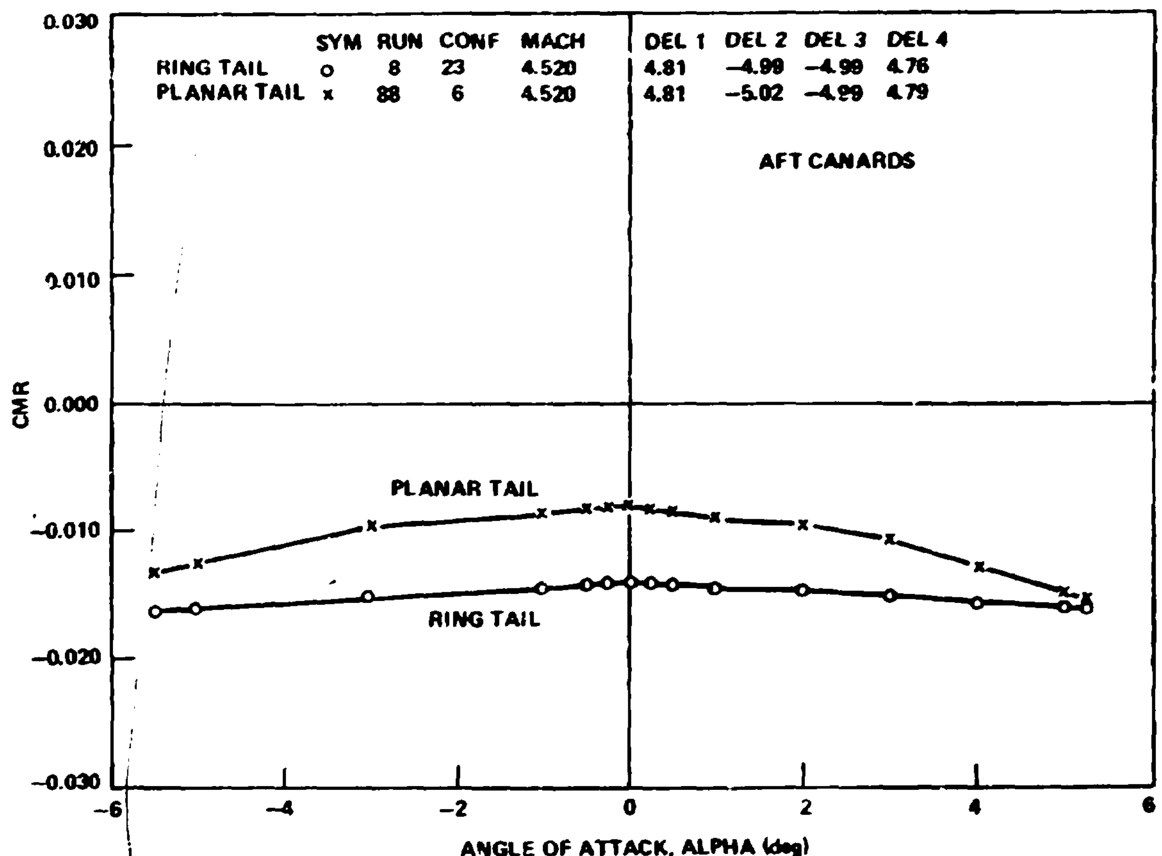

Figure 49. Total rolling moment coefficient versus angle of attack, $M_\infty = 4.5$, planar tail, ring tail.

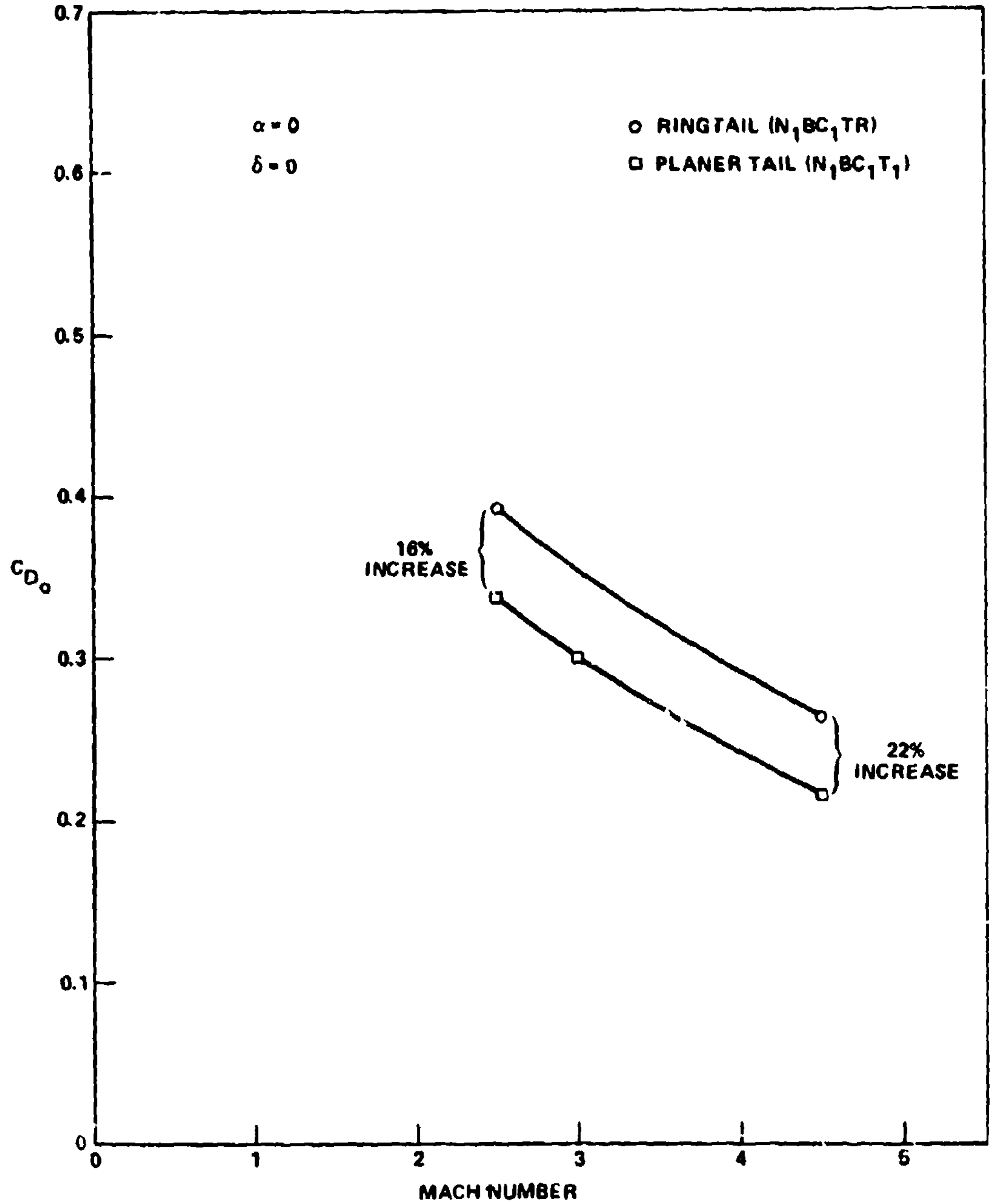

Figure 50. Change in drag due to ring tail.

REFERENCES

1. Free Flight Rocket Technology Program Aeroballistics Directorate FY-74 Activity Report, US Army Missile Command Technical Report No. TR-RD-75-3, July 1974.

2. Pitts, W. C., Neilsen, J. N., and Kaattari, G. E., Lift and Center of Pressure of Wing-Body-Tail Combinations at Subsonic, Transonic, and Supersonic Speeds, NACA Report 1307, 1959.

3. 8-Foot Transonic Wind Tunnel, CALSPAN Corporation Wind Tunnel Report No. WTO-300, Revised October 1971.

4. Burt, J. R., Jr., An Experimental Investigation of the Aerodynamic Characteristics of Several Nose-Mounted Canard Configurations at Transonic Mach Numbers, US Army Missile Command Technical Report RD-75-2, August 1974.

5. Burt, J. R., Jr., An Experimental Investigation of the Aerodynamic Characteristics of Several Nose-Mounted Canard Configurations at Supersonic Mach Numbers, US Army Missile Command Technical Report RD-75-17, January 1975.

6. Burt, J. R., Jr., An Experimental Investigation of the Aerodynamic Characteristics of Nose Mounted Canard Configuration at Supersonic Mach Numbers (1.5 through 4.5), US Army Missile Command Technical Report RD-77-5, October 1976.

7. Spahr, J. R., and Dickey, R. R., Wind-Tunnel Investigation of the Vortex Wake and Downwash Field Behind Triangular Wings and Wing-Body Combinations at Supersonic Speeds, NACA RMA53D10, June 1953.

LIST OF SYMBOLS

A	Reference area, maximum body cross section, 19.63 in.^{2}
$C_{M_{B_{Cx}}}$	Root bending moment coefficient for canard No. x, $M_{B_{Cx}}/QAD$
$C_{M_{B_{Tx}}}$	Root bending moment coefficient for tail No. x, $M_{B_{Tx}}/QAD$
C_{M_R}	Model rolling moment coefficient
$C_{M_{R_C}}$	Rolling moment coefficient due to canards only, M_{R_C}/QAD
$C_{M_{R_o}}$	Model rolling moment coefficient with undeflected canards
$C_{M_{R_T}}$	Rolling moment coefficient due to tails only, M_{R_T}/QAD
$C_{N_{Cx}}$	Normal force coefficient for canard No. x, N_{Cx}/QA
$C_{N_{Tx}}$	Normal force coefficient for tail No. x, N_{Tx}/QA
D	Body maximum diameter, reference diameter, 5.0 in.
M_∞	Free stream Mach number
$M_{B_{Cx}}$	Root bending moment for canard No. x
$M_{B_{Tx}}$	Root bending moment for tail No. x
M_{R_C}	Rolling moment due to canards only
M_{R_T}	Rolling moment due to tail only
N_{Cx}	Normal force for canard No. x
N_{Tx}	Normal force for tail No. x
Q	Dynamic pressure, $1/2\ \rho V^2$, lb/ft^2

R_C	Body radius at the canard hinge point
R_T	Body radius at the tail hinge point
V_∞	Free stream velocity
x	Canard or tail panel number
α	Angle of attack (deg)
δ_{Cx}, DEL_x DEL_x	Deflection angle for canard No. x (deg)
ρ	Free stream density

DISTRIBUTION

	No. of Copies
Defense Documentation Center Cameron Station Alexandria, Virginia 22314	6
Commanding General US Army Materiel Development and Readiness Command Research and Development Directorate ATTN: DRCRD Washington, D.C. 20315	1
Commanding Officer US Army Picatinny Arsenal ATTN: SMUPA-VC3, Mr. A. Loeb Dover, New Jersey 07801	1
Director US Army Mobility Research and Development Laboratory ATTN: SAVDL-AS Ames Research Center Moffett Field, California 94035	1
Commanding Officer Research Laboratories ATTN: SMUEA-RA, Mr. Abraham Flatau Edgewood Arsenal, Maryland 21010	1
Commanding Officer Air Force Armament Laboratory ATTN: Mr. C. Butler Mr. F. Howard Dr. F. Findley Eglin Air Force Base, Florida 32542	 1 1 1
Arnold Engineering and Development Center ATTN: Dr. McKay Library Arnold Air Force Station, Tennessee 37389	 1 1
Air Force Flight Dynamics Laboratory ATTN: FDMM, Mr. Gene Fleeman Wright-Patterson Air Force Base, Ohio 45433	1
Commanding Officer Ballistic Research Laboratories ATTN: AMXRD-BEL, Mr. R. Krieger Aberdeen Proving Ground, Maryland 21005	1
Commanding Officer US Naval Ordnance Laboratories ATTN: Mr. S. Hastings Mr. R. T. Hall Library White Oak Silver Springs, Maryland 20910	 1 1 1
NASA-Langley Research Center ATTN: Mr. Leroy Spearman Mr. Charles Jackson Technical Library Langley Field, Virginia 23365	 1 1 1
Commanding Officer and Director Naval Ship Research and Development Center ATTN: Aerodynamic Laboratory Carderock, Maryland 20007	1
Naval Weapons Center ATTN: Mr. R. Meeker China Lake, California 93555	1

	No. of Copies
NASA-Ames Research Center ATTN: Technical Library Moffett Field, California 94035	1
NASA-Lewis Research Center ATTN: Technical Library Cleveland, Ohio 44135	1
NASA-Marshall Space Flight Center ATTN: Technical Library Marshall Space Flight Center, Alabama 35812	1
US Air Force Academy ATTN: Lt. Col. W. A. Edington, DFAN USAF Academy, Colorado 80840	1
Philco Corporation Aeronutronic Division ATTN: Technical Information Services - Acquisitions Mr. L. E. Horowitz Ford Road Newport Beach, California 92663	1
Rockwell International Columbus Aircraft Division ATTN: Mr. Fred Hessman 4300 East Fifth Avenue Columbus, Ohio 43216	1
Sandia Corporation Sandia Base Division 9322 ATTN: Mr. W. Curry Box 5800 Albuquerque, New Mexico 87115	1
Purdue University ATTN: Dr. J. Hoffman, Propulsion Center Lafayette, Indiana 47907	1
University of Alabama Department of Aerospace Engineering ATTN: Dr. Zien Dr. J. O. Doughty University, Alabama 35486	 1 1
Jet Propulsion Laboratory California Institute of Technology ATTN: Mr. R. Martin 4800 Oak Grove Drive Pasadena, California 91109	1
University of Missouri at Columbia Department of Mechanical Engineering ATTN: Dr. D. E. Wollersheim Columbia, Missouri 65201	1
University of Illinois College of Engineering ATTN: Dr. A. L. Addy Dr. H. H. Korst Dr. R. A. White Engineering Library Urbana, Illinois 61801	 1 1 1 1
Johns Hopkins University Applied Physics Laboratory ATTN: Dr. L. Cronvich Mr. Gordon Dugger Mr. R. Walker 8621 Georgia Avenue Silver Springs, Maryland 20910	 1 1 1

	No. of Copies
University of Notre Dame	
Department of Aerospace Engineering	
ATTN: Dr. T. J. Mueller	1
Notre Dame, Indiana 46556	
Boeing Company	
ATTN: Library Unit Chief	1
Mr. R. J. Dixon	1
Mr. H. L. Giles	1
PO Box 3707	
Seattle, Washington 98124	
Convair, A Division of General Dynamics Corporation	
ATTN: Division Library	1
Pomona, California 91776	
Nielsen Engineering and Research, Inc.	
ATTN: Dr. Jack N. Nielsen	1
850 Maude Avenue	
Mountain View, California 940-0	
Hughes Aircraft Company	
ATTN: Documents Group Technical Library	1
Florence Avenue at Teale Street	
Culver City, California 90230	
Ling-Temco-Vought Aerospace Corporation	
ATTN: Mr. Dick Fillison	1
PO Box 404	
Warren, Michigan 48090	
Ling-Temco-Vought Aerospace Corporation	
Vought Aeronautics Division	
ATTN: C. R. James, Unit 2-53330	1
Box 5907	
Dallas, Texas 75222	
Lockheed Missiles and Space Company	
Huntsville Research and Engineering Center	
ATTN: Mr. J. Benefield	1
4800 Bradford Boulevard, NW	
Huntsville, Alabama 35805	
Lockheed Aircraft Corporation	
Missile and Space Division	
ATTN: Technical Information Center	1
PO Box 504	
Sunnyvale, California	
The Martin-Marietta Corporation	
Orlando Division	
ATTN: D. Tipping	1
L. Gilbert	1
Orlando, Florida 32804	
McDonnel-Douglas Company-West	
ATTN: Library A3-328	1
5301 Bolsa Avenue	
Huntington Beach, California 92646	

	No. of Copies
McDonnel-Douglas Corporation	
PO Box 516	
St. Louis, Missouri 63166	1
Northrop Corporation	
Electro-Mechanical Division	
ATTN: Mr. E. Clark	1
500 East Orangethrope Y20	
Anaheim, California 92801	
Emerson Electric Company	
ATTN: Mr. Robert Bauman	1
8100 Florissant	
St. Louis, Missouri 73136	
Data Management Services	
Department 2910	
Chrysler Corporation Space Division	
ATTN: Mr. N. D. Kemp	6
PO Box 29200	
New Orleans, Louisiana 70189	
Data Management Services	
Department 5307	
Chrysler Corporation	
Huntsville Electronics Division	
ATTN: Mr. J. E. Vaughn	1
102 Wynn Drive	
Huntsville, Alabama 35805	
DRSMI-FR, Mr. Strickland	1
-LP, Mr. Voigt	1
-R, Dr. McDaniel	1
Dr. Kobler	1
-RBD	3
-RKD, Mr. Deep	1
Mr. Burt	15
-RPR (Record Set)	1
(Reference Copy)	1